Titre: Title:	Indoor Localization Using Channel State Information with Regression Artificial Neural Network
Auteur: Author:	Seyed Mohsen Samadani
Date:	2019
Type:	Mémoire ou thèse / Dissertation or Thesis
Référence: Citation:	Samadani, S. M. (2019). Indoor Localization Using Channel State Information with Regression Artificial Neural Network [Mémoire de maîtrise, Polytechnique Montréal]. PolyPublie. https://publications.polymtl.ca/4176/

URL de PolyPublie: PolyPublie URL:	https://publications.polymtl.ca/4176/
Directeurs de recherche: Advisors:	Chahe Nerguizian, & Yvon Savaria
Programme: Program:	génie électrique

POLYTECHNIQUE MONTRÉAL

affiliée à l'Université de Montréal

Indoor localization using channel state information with regression artificial neural network

SEYED MOHSEN SAMADANI

Département de génie électrique

Mémoire présenté en vue de l'obtention du diplôme de Maîtrise ès sciences appliquées

Génie électrique

Décembre 2019

POLYTECHNIQUE MONTRÉAL

affiliée à l'Université de Montréal

Ce mémoire intitulé :

Indoor localization using channel state information with regression artificial neural network

présenté par **Seyed Mohsen SAMADANI**

en vue de l'obtention du diplôme de *Maîtrise ès sciences appliquées*

a été dûment accepté par le jury d'examen constitué de :

Christian CARDINAL, président

Chahé NERGUIZIAN, membre et directeur de recherche

Yvon SAVARIA, membre et codirecteur de recherche

Francois LEDUC-PRIMEAU, membre

ACKNOWLEDGEMENTS

First, I would like to express my sincere gratitude and appreciation to my supervisor and co-supervisor Prof. Chahé Nerguizian and Prof. Yvon Savaria for their useful advices, patience, encouragement and support during my M.Sc.A program.

Having their help throughout all steps of this research from financial support and explaining the very first idea of the research to introducing helpful staff and giving endless hints and directions made it possible to achieve the research goals.

I also would like to offer my cordial thanks to Saad Chidami, Jean-Sébastien Décarie and all my friends who gave me their time and practical advices and assistance to solve technical problems and move forward.

Finally yet importantly, my special thanks go to my parents and my siblings for their continuous encouragement and unconditional love.

RÉSUMÉ

Dans cette recherche, les informations sur l'état du canal (CSI) sont utilisées pour localiser les stations mobiles dans un environnement intérieur. À cette fin, deux ordinateurs portables équipés de la carte Intel Wireless Wi-Fi Wireless Link 5300 disponible dans le commerce sont utilisés. Les informations CSI sont collectées en établissant une connexion sans fil entre deux machines de plus de 200, 70 et 52 points de référence (RP) aux sixième, cinquième et troisième étages respectivement, dans l'immeuble Lassonde de Polytechnique Montréal servant de banc d'essai expérimental.

Différentes approches de localisation sont étudiées et comparées les unes aux autres en termes de précision de localisation. Dans la première approche, les CSI collectés alimentent directement le réseau de neurones artificiels (RNA) en tant que caractéristiques d'entrée et le RNA appris est utilisé en tant qu'algorithme de correspondance du modèle afin de prédire la position de l'utilisateur. La deuxième approche consiste à appliquer à l'entrée de RNA les paramètres pertinents du canal extrait représentant le nombre réduit d'entités à l'entrée de RNA. Enfin, une exploration est effectuée pour trouver la meilleure configuration de couches cachées et de facteurs d'étalement pour les réseaux Perceptron multicouche (MLP) et Réseaux de neurones à régression générale (GRNN), respectivement.

ABSTRACT

In this research, the Channel State Information (CSI) is leveraged to locate mobile stations in an indoor environment. For this purpose, two laptops equipped with the off-the-shelf Intel Wi-Fi Wireless Link 5300 (NIC card) are used. CSI information is collected by establishing a wireless connection between two machines over 200, 70 and 52 reference points (RP) on sixth, fifth, and third floors respectively, in Lassonde building of Polytechnique Montreal as the experimental testbed.

Different geolocation approaches are investigated and compared with each other in terms of location accuracy and precision. In the first approach, the collected CSIs are directly fed to the artificial neural network (ANN) as input features and the learned ANN is used as the pattern-matching algorithm in order to predict the user's location. The second approach consists in applying at the input of the ANN the extracted channel relevant parameters representing the reduced number of features at the input of ANN. Finally, exploration is performed to find the best configuration of hidden layers and spread factors for Multilayer Perceptron (MLPs) and General Regression Neural Networks (GRNNs), respectively.

TABLE OF CONTENTS

LIST OF TABLES

LIST OF FIGURES

LIST OF ACCRONYMS AND ABREVIATIONS

Localization-Based Services (LBS)

Global Positioning System (GPS)

Non-Line of Sight (NLoS)

Line of Sight (LoS)

Indoor Positioning Systems (IPS)

Angle of Arrival (AoA)

Time of Arrival (ToA)

Received Signal Strength (RSS)

Received Signal Strength Indicator (RSSI)

Channel State Information (CSI)

Medium Access Control (MAC)

Physical layer (PHY)

Channel Frequency Response (CFR)

Transmitter antennas (Tx)

Receiver antennas (Rx)

Orthogonal Frequency Division Multiplexing (OFDM)

Multiple Inputs Multiple Outputs (MIMO)

Radio Frequency (RF)

Infrared Radiation (IR)

Time Difference of Arrival (TDoA)

Angle of Arrival (AoA)

Inertial Measurement Unit (IMU)

Degrees of Freedom (DOF)

Pedestrian Dead Reckoning (PDR)

Light-Emitting Diode (LED)

Radio-Frequency Identification (RFID)

Ultra-Wide Band (UWB)

Support Vector Machine (SVM)

Bluetooth Low Energy (BLE)

Magnetic Matching (MM)

Ultra-Wide Band (UWB)

Target Node (TN)

Anchor Node (AN)

Time Difference of Arrival (TDoA)

Access Point (AP)

Principal Component Analysis (PCA)

K-Nearest Neighbors (KNN)

Angle of Departure (AoD)

Return Time of Flight (RToF)

Time of Flight (ToF)

Inverse Fourier Transform (IFT)

Channel Impulse Response (CIR)

Multi-Layer Perceptron (MLP)

Artificial Neural Network (ANN)

General Regression Neural Networks (GRNN)

Energy of the Direct Path (EDP)

Angle of the Direct Path (ANDP)

Power Delay Profile (PDP)

Detecting Point (DP)

K-Nearest Neighbor (KNN)

Restricted Boltzmann Machine (RBM)

First Fresnel Zone (FFZ)

Uniform Circular Array (UCA)

Root Mean Square Error (RMSE)

Effective Coverage Range (ECR)

Convolutional Neural Network (CNN)

Deep Convolutional Neural Network (DCNN)

Deep Neural Network (DNN)

Fingerprinting (FP)

Feedforward network (FFN)

Long Short-Term Memory networks (LSTM)

Modulation and Coding Scheme (MCS)

Discrete Wavelet transform (DWT)

LIST OF APPENDICES

CHAPTER 1 INTRODUCTION

In this chapter, localization-based services (LBS) systems together with frequently used technologies, and techniques of indoor positioning are addressed, followed by the outline of this research.

1.1. Localization based services

Localization-based services (LBS) systems play an increasingly significant role in our everyday life. Both outdoor and indoor LBS systems are getting ever-progressing attention for their contribution to a wide range of services that they can provide related to locating objects or people relative to a reference point. Some well-known examples of outdoor services are Google Maps, Waze, Uber, etc. As for indoor services, one may consider some LBSs such as indoor navigation in airports, touristic sites, tracking customer movement patterns in big shopping malls to improve advertisement, security, disaster management, etc. Indoor LBS particularly needs more technological innovations and advancement since the traditional Global Positioning System (GPS) fails to function accurately inside buildings for two reasons namely multipath and non-line of sight (NLOS) paths.

1.2. Problem Definition and Purpose

The complex structure of indoor environments results in multiple copies of reflected signals known as multipath on one hand, and on the other hand, obstacles such as furniture and walls eliminate the line of sight (LOS) path, which consequently leads to the fading phenomenon. Therefore, as previously mentioned, new alternative approaches are needed to improve the functionality of indoor positioning systems (IPS).

Various methods mostly relying on WiFi, have been adopted in an attempt to constantly ameliorate the indoor localization performance, which falls in two major categories, namely signal geometric-based and fingerprinting-based approaches. The former deal with physical metrics of a signal, such as the angle of arrival (AoA), time of arrival (ToA), received signal strength (RSS), channel state information (CSI) and determine the position of the target using geometric calculations. The latter processes the same physical metrics to extract the best representative features of a location to create a database containing the related features of all locations. Most of the previous researches have been done using RSS, a measure from the Medium Access Control

(MAC) layer, which is low-resolution information due to having only one measurement per transmission. Moreover, RSS may be affected by people in an indoor environment and by reflected copies of itself to undergo fading which results in a lower degree of reliability.

Unlike RSS, which is coarse-grained information, a new measure with a very rich package of information has been introduced recently, known as CSI.

CSI is a feature of the physical layer (PHY), in fact the sampled version of channel frequency response (CFR), which contains complex values representing the amplitudes and phases response of communication links between transmitter antennas (Tx) and receiver antennas (Rx) over 30 orthogonal frequency division multiplexing (OFDM) subcarriers.

This fine-grained information makes it possible to analyze the WiFi channel in terms of its frequency selective characteristics together with having valuable information for each subcarrier and consequently a more reliable performance in localization. Both RSS and CSI have been used in signal spatial feature-based and fingerprinting-based approaches. The CSI metric has attracted increasing attention in recent years though, due to its richness, its availability in on off-the-shelf Network Interface Card (NIC) and its robustness as it is almost time-independent and shows an acceptably steady behavior.

Leveraging CSI method was developed by Halperin et al. [1] to predict whether communication link will have a successful performance in packet delivery, by introducing the use of channel measurements reported by commodity 802.11n NIC to support beamforming in multiple inputs multiple outputs (MIMO) streams.

1.3. Technologies

Frequently used technologies, including non-Radio Frequency-based and Radio Frequency-based (RF-based) in localization, are addressed in this section.

1.3.1. Non-RF Technologies

Among non-RF technologies, the following can be mentioned: Sound, Infrared Radiation (IR), Inertial Sensors, Geomagnetic, Ultrasound, and Visible light.

Sound-based localization methods can be broadly categorized into two groups, namely Time Difference of Arrival (TDOA) and Angle of Arrival (AoA). In TDOA the recorded sound arrived

from multiple transmitters, is sent to a data fusion center where positioning is done using a triangulation algorithm considering the signal time differences at the target's location. In AoA approaches, the angle of arrival at each receiver node is calculated for all locations to make a fingerprint of the testbed. Some examples of sound-based approaches are presented in references [1, 2, 3].

In IR-based localization, an IR tag is attached to the target, and this tag emits a signal to the network of receivers, which are in charge of determining the location of the target. One of the earliest researches using IR technology has been carried out in [4] to locate the staff in an organization by making them wear a badge, which sends IR beacon at an interval of 15 seconds. Due to its need for a line of sight and a large number of receivers resulted from the short-range of IR signals, this technology is gradually losing its popularity despite its accuracy; although it is still used in some researches [5, 6]. Since the emphasis in this research is on the RF-based approach, we do not go farther and refer the reader to the aforementioned references.

Inertial Sensors-based approaches take advantage of Inertial Measurement Unit (IMU) sensors, usually available on smartphones. An IMU is a sensor with 2 to 6 Degrees of Freedom (DOF) which detects the direction of the movement, the distance and the steps taken to track the target and calculate its position, here the phone holder. The references [7, 8, 9, and 10] employed this approach.

Another technology, which is used in positioning, is the geomagnetic field signal. Two examples of this approach are implemented in reference [11] and [12]. In the former, the system collects the intensity of the magnetic field of every location to make a fingerprinting database of the testbed. Then to locate a user it is enough to take some steps carrying a smartphone and the system locates the target by integrating the fingerprint map with pedestrian dead reckoning (PDR), received from the smartphone by Kalman filter. The latter uses the distortion of the magnetic field and with the help of the extended Kalman filter, it locates a robot, which is equipped with a geomagnetic sensor.

Ultrasound-based technology localizes the target by means of ultrasonic transmitter and receiver nodes and Dead Reckoning as in [13] and unsynchronized ultrasound senders on the ceiling with a target equipped with ultrasound receiver in [14]. Another research is presented in

reference [15] in which, the smartphone as the receiver listens and records constantly and through 3 steps of filtering, pilot detection, and fine decoding, identifies in which room it is.

As a Visible light-based approach, reference [16] benefits from Light-emitting diodes (LEDs) to transform the encoded IDs (by LED controller) received from the server to optical signals. On the other side, the optical receivers transform the optical signal to an electrical signal, which will be received through the MIC jack of a smartphone to be decoded. Finally, the location is obtained from the server by implementing the proximity technique.

1.3.2. RF Technologies

RF technologies utilized in indoor localization are as follows. Bluetooth, Radio-Frequency Identification (RFID), Ultra-Wide Band (UWB) and Wi-Fi.

Reference [17] employs a crowdsourcing method, which is based on the Support Vector Machine (SVM) classification algorithm, by using smartphone sensors, to generate Bluetooth Low Energy (BLE) landmarks in the training phase. Moreover, to achieve higher performance in the localization phase it implements a particle filter to fusion PDR and the results of landmark detection to reduce the cumulative error of PDR. Another research [18] takes advantage of RSSI to perform indoor localization. It also adds two self-adaptive filters, namely smoothing and wavelet filters, to overcome the inherent instability of the BLE signal as well as de-noising it. Finally, the position of the target is identified by using the equation of path loss model-based RSSI.

RFID-based indoor localization has been studied and carried out in reference [19] using an active RFID tag and an RFID reader. The localization is done by employing the log-distance path loss model. Reference [20] presents an RFID-based technique combined with Pedestrian Dead Reckoning (PDR) and Magnetic Matching (MM) technologies, in which, the fingerprint of the testbed is constructed using the dual-frequency RFID. The target person who carries a tag including a gyroscope, acceleration sensor, and magnetic sensor walks in the testbed and simultaneously these data are received by RFID readers. To reach an accurate estimation of a person’s step size the author suggests fusing the RSS to the floor map. Finally, a particle filter merges the three aforementioned technologies to localize the target.

Ultra-Wide Band (UWB) is another RF-based technology used in several types of research such as reference [21] where a target node (TN) is tracked while moving in a corridor by means of

four uniformly positioned fixed anchor nodes (ANs) and an analytical approach to minimize the estimation error of localization. Since the ANs and TN are not synchronized, the time difference of arrival (TDOA) is considered as localization technique. TN can localize itself upon receiving signals from four ANs, either onboard or on a server that receives the TN data. Reference [22] presents a localization algorithm, based on two ways time of flight to estimate the distance between the transmitter and the receiver. The system works as follows, a signal at a specific time Ta1 is sent from device A to devise B where the signal is received at Ta2. The received signal will be sent back to devise A after a specific time. This way by calculating the whole ToF, the distance between the two transceivers will be determined.

Wi-Fi is the most popular RF technology, used in localization, due to its availability on electronic devices such as laptops and smartphones and the possibility of employing access points (APs) as the anchors. In reference [23] a received signal strength (RSS)-based fingerprinting technique is adopted. In the offline phase, by choosing specific locations known as reference points, raw RSS is collected on a known time interval, from the APs to the mobile device, located in different directions. Then the fingerprinting map is constructed using the average of received RSS time samples. In the online phase, the RSS is compared to the fingerprinting map using the nearest neighbor method to find the location of the target.

Reference [24] presents an RSSI-based fingerprinting approach in which they collected RSSI over 45 points, from six APs at the offline stage, using an application on a smartphone. Then, the collected data is processed by the Principal Component Analysis (PCA) for dimension reduction and feature extraction. Finally, a classification is used choosing one of the four classifiers namely, K-Nearest Neighbors (KNN), Decision Tree, Random Forest, and SVM to build the radio map. At the test phase, two experiments have been conducted. In the first one, a static point is located and in the other test, a dynamic positioning for a trajectory is performed.

1.3.3. Techniques of indoor localization

Two distinct techniques have been widely used in indoor positioning literature, namely geometric and mapping. In the former signal features such as received signal strength indicator (RSSI), parameters related to time including ToA and TDoA, signal angle features like angle of arrival (AoA) and angle of departure (AoD), or channel state information (CSI), are employed to localize the target using trilateration and triangulation methods. The latter techniques are also

known as fingerprinting, use the signal features at the offline phase to construct a radio map consisting of processed signal features together with the coordinates of each point of measurement.

1.3.4. Techniques based on RSSI

In RSSI-based techniques, the target is localized using the RSSI, which is received at several receivers, typically the access points (APs), and triangulation/trilateration methods. Depending on the received RSSI, the radius in which the target is located can be determined by adding two more reference points and by finding the intersection of three circles, the system is able to pinpoint the target. Some examples of RSSI-based localization are given in [25] and [26]. In practice, the RSSI is not stable over time and it is dependent on the environmental structure and consequently the multipath phenomenon.

1.3.5. Techniques based on time

In these approaches, the process of localization is based on the duration of time. The distance is calculated with regard to the signal return time of flight (RToF), from multiple APs to the target and its return time, time of flight/arrival (ToF/ToA) which is the time that it takes for the signal from the target, to reach the receiver. Alternatively, the time difference of arrival (TDoA) in which the time difference of signal reception at two precisely time-synchronized receivers is considered to localize the target. Obviously, the time synchronization is essential for these systems, to have an accurate target positioning. References [27, 28] presents researches using the time-based localization.

1.3.6. Techniques based on angle

The angle of arrival (AoA) is the angle at which the RF wave reaches the antenna of a receiver. By taking advantage of multiple antennas with known distance from each other on an antenna array, it is possible to calculate the AoA by means of TDoA on each antenna. This technique can be implemented jointly with other metrics such as ToF and RSSI. These systems need multiple antennas, which means that more hardware is needed. Moreover, in the case of multipath, the calculation of AoA becomes complicated. References [29, 30] present some localization systems, which use AoA-based technology.

1.3.7. Techniques based on CSI

Channel State Information (CSI) can be described as a package, which contains information related to the communication channel between transmitter (Tx) and receiver (Rx). This information presents the state of the channel in the frequency domain as a complex value, over 30 sub-carriers for each Tx-Rx link. Depending on the setting of communication parameters, it is possible to choose the number of Tx and RX antenna. References [31, 32] employ the CSI technique for indoor localization.

1.3.8. Techniques based on mapping

Mapping or fingerprinting techniques employs unique physical features such as RSSI, AoA, CSI, related to each point of measurement at the training phase, and after some data processing, constructs a database. This database is used at the test phase to estimate the location, related to a new measurement from the testbed. Some mapping/fingerprinting-based researches are as follows, references [33, 34]. The process of surveying the testbed to collect data for the training phase is laborious and due to changes in the structure and arrangement of the interior design of indoor environments, the database should be updated after any change.

There are some methods, which are used in the mapping stage, such as probabilistic, neural network, SVM, KNN, etc.

1.4. Objectives

This research is mostly inspired by the approach of exploiting the channel impulse response, introduced in [35] where a frequency channel sounder is used to get the transfer function of a complex channel in an underground gold mine. Then, by applying the Inverse Fourier Transform (IFT), the Channel Impulse Response (CIR) is obtained for 490 measurement points. From the obtained 490 CIRs, seven wireless channel relevant parameters are extracted and used as fingerprints for the input of MLP and GRNN neural networks with the aim to locate miners in case of accidents. In this experiment, the objective is to reach the sub-meter localization accuracy using CSI as the fingerprinting information and the artificial neural network as the mapping algorithm.

The novelty of our technique is using multiple packets of CSI for each location without feature extraction to provide a reach fingerprint. Two different mapping algorithms are investigated and compared with each other in terms of location accuracy and precision. In the first

approach, the collected CSIs are fed to the multilayer perceptron (MLP) as input features and the learned artificial neural network (ANN) is used as the pattern-matching algorithm in order to predict the user's location. The second approach uses General Regression Neural Networks (GRNN). Finally, exploration is performed to find the best-hidden layer configuration and spread factors for Multilayer Perceptrons (MLPs) and General Regression Neural Networks (GRNNs), respectively.

1.5. Research Outline

The outline of this research is as follows, chapter two gives a review of the state of the art, and then in chapter three the methodology and the detailed approach are introduced. Finally, in chapter four, we examine the experimental results followed by the evaluation of the approach.

CHAPTER 2 LITERATURE REVIEW

In this chapter, some background for indoor localization and review of the state-of-the-art methods, specifically based on CSI, are presented which can be broadly categorized into groups of geometric-based and fingerprinting-based approaches.

The technique to collect CSI was introduced for the first time in 2011 in reference [36] by Daniel Halperin et al. The motivation for their technique was to find a way to obtain detailed information including the behavior of the communication channel between each pair of transmitter and receiver over a specific number of subcarriers. This detailed information, which is extracted from the physical layer, compared to RSSI with only the received signal power, contains more information about the variations of the channel and is used to improve the performance of the wireless network. In their work, they used the commodity WiFi Link 5300 wireless NIC and a modified firmware to get access to the CSI report, which is included in a packet preamble, based on the IEEE 802.11n standard. This information is originally considered to remove the variations caused by the channel to ameliorate the functionality of its communication.

The first research about localization using CSI is done in reference [37], which is a geometrical-based method. FILA uses effective CSI data and trilateration to perform localization. First, to decrease the effect of multipath, it takes CSI data and applies IFFT on it to convert it and obtain the channel response in the time domain. Bandwidth limitation makes it difficult to identify every signal paths, instead only clusters of paths are distinguishable. The first cluster is assumed to contain either the LOS or the NLOS for the shortest path. To keep the first cluster and remove the others, a truncation window with a threshold at 50% is used to filter out other clusters and counteract the error caused by reflection. Then by applying FFT, CSI is converted back into the frequency domain. Moreover, to compensate for the effect of selective fading caused because the coherence bandwidth of the channel is smaller than the bandwidth of the signal, the weighted average of 30 groups of CSIs is used to improve the system accuracy. Consequently, to relate the distance and the effective CSI, a modified indoor propagation model is developed. In addition, to simplify the calculation, FILA assumes that an equal path loss exponent is affecting the signal traveling between three APs and the target and considers a specific environment factor. Following the developing of the model, supervised learning is done by collection CSIs at two APs and training the system to retrieve the path loss exponent and the environment factor, and then a third AP comes

in the picture to perform the test. The process continues until real parameters and estimated ones converge. Finally, at the localization phase, the distance between the target and the APS is calculated using the CSI received at APs and the parameters obtained resulted from the training phase, at a specified receiver. All APs send their coordinates together with the received effective CSIs to a specified receiver, where the receiver aggregates the effective CSIs and performs the trilateration method using the calculated distances to locate the target. The median accuracy of FILA is 0.45m and 1.2m in an anechoic chamber and a laboratory, respectively.

In reference [38], which is a fingerprinting-based method, CSI information is used to make the radio map and with the help of a probability algorithm, the location of the target is determined. The functionality of the proposed method, Fine-grained Indoor Fingerprinting System (FIFS) is composed of two main phases, calibration, and positioning. In the calibration phase, it takes raw CSIs, which are collected by an HP laptop from three APs for each location, and generates the fingerprint. For this reason, they averaged CSIs over all the antennas and considering the coherence bandwidth of the subcarriers, they defined four sub-bands. Each of these sub-bands contains a group of subcarriers with maximum similarity. If the frequency distance between two sub-carrier is lower than the coherence bandwidth, they belong to the same sub-band. The idea of defining sub-bands indicates the aspect of fading. In other words, fading happens independently among subcarriers from different sub-bands so the frequency diversity can be taken into account. In the positioning phase, a probabilistic approach is adopted as the mapping algorithm due to its higher accuracy. FIFS shows an acceptable performance with a 1m mean error. Considering the results, FIFS achieves a successful localization with the mean error slightly under one meter.

In CUPID [39], CSI data is combined with displacement of the target to identify the direct path and localize the target by calculating the distance between the AP and the target in two different locations and the AoA related to each location. Two concepts are addressed, namely the energy of the direct path (EDP) and the angle of the direct path (ANDP). CUPID applies IFFT on the received CSIs to convert them from frequency to time domain and find the power delay profile (PDP). It assumes that due to the resolution of PDP, which is equal to 50ns for 20MHz 802.11n, the first component of PDP can be considered as the container of the EDP and the other components have traveled a longer distance of +15m regarding the 50ns resolution of PDP. At the same time, another parameter called LoSfactor, which is the proportion of EDP to RSSI, is computed at the AP. Having the EDP and the LoSfactor, the correct path loss exponent is selected

to be used in the calculation of the distance. The AP tracks the target that moves from location A to B and determines the variation of ANDP by taking advantage of the accelerometer and the gyroscope of the mobile client, as well as the AoA, measured at two locations to build up the pseudo spectrum. In the pseudo spectrum, the AoA, which remains unchanged, is considered as the direct path. Finally, the estimated location of the target is equal to the coordinates of the AP plus the distance in y and x directions by applying the ANDP. CUPID shows a median localization error of 2.7m.

Another research using CSI in localization is presented in reference [40]. Unlike conventional indoor localization systems, Pilot does not track the target rather it determines the potential presence of entities in an environment of interest. Its functionality is based on the detection of any perturbation caused to the CSI fingerprint of an area by the presence of an entity, thus passive localization. The pilot is composed of three parts, APs, detecting points (DPs), and the server. The APs constantly broadcast to DPs, where the transmitted messages are stored and transferred to the server. At the server, the received messages are processed and if no anomaly detected, they will be used to construct the passive radio map, otherwise, if any shift in the pattern of the CSI features exists, the server stores them in an abnormal database. The block that detects the anomaly, constantly calculates the variance of newly received CSIs with regard to previous CSIs to realize if any change happened. If it notices abnormal CSI features, the positioning block appears to map the new CSI with coordinates stored in the database of abnormal CSI to locate the entity. To detect the abnormality, the kernel density estimation (KDE) approach is adopted to examine the cumulative distribution function (CDF) of the CSI correlation. It detects the abnormality when the sample correlation is less than a predefined lower bound. As for the mapping, Pilot uses a probabilistic algorithm known as maximum a priori probability (MAP) algorithm to estimate the entity location. Pilot proves to outperform RASID (the RSS based system) by around 10%.

Reference [41] introduces a fingerprinting-based method, called CSI-MIMO, which leverages MIMO information together with the amplitude and the phase of CSI data. The aggregation of CSI data from multiple antennas and subcarriers is used to build up the radio map for multiple APs, and with K-nearest neighbor (KNN), the functionality of it is confirmed. At the training phase, CSIs packets sent by an AP are collected at 19 reference points for 24 hours. Then the amplitude and the phase of each subcarrier are subtracted from those of the next subcarrier to

make the CSI-MIMO fingerprint for each location, and the whole locations' fingerprint is stored in the database. Then, at the positioning phase at an unknown location, CSI is collected and the same process as in the training phase is done to get its fingerprint. CSI-MIMO compares the new fingerprint with the database by means of deterministic and probabilistic approaches, KNN and maximum likelihood estimation, respectively. CSI-MIMO achieves the mean distance error of 0.95 m.

Reference [30] presents the SpotFi system, which takes advantage of super-resolution algorithm to calculate jointly the AoA and the time of flight (ToF) of multipath components of collected CSI and RSSI at each AP. It also determines the AoA of the direct path by presenting a new filtering and estimation technique. Spotfi overcomes the limited number of antennas by creating a virtual sensor array with a higher number of elements compared to multipath components. As the presence of multipath makes difficult the determination of the L paths' AoA while the number of antennas is three, Spotfi implements super-resolution, a method, based on MUSIC algorithm. MUSIC algorithm, defines the received signal X on each sensor (here antenna), as the multiplication of the matrix A of steering vectors, which are the phase shifts on the array of antennas, due to the distance between them, and the matrix F of complex attenuation vectors. Based on MUSIC, if we find the eigenvectors of XXH, which correspond to the eigenvalue of zero or in other words orthogonal to steering matrix A, we can compute A and consequently, AoA can be found. However this algorithm needs a condition to be satisfied, matrix A has to be skinny (more rows than columns) and matrix F should be fat (more column than rows) to work correctly. More rows than columns can be translated to more sensors than propagation paths, however, with only three antennas on Intel 5300, this algorithm fails to work. This is where Spotfi solves the problem by the super-resolution estimation. The main idea of Spotfi is that the limitation of antennas can be overcome by considering the subcarriers' number time the number of antennas, which gives 30 x 3 =90 sensors. Since the phase shift, among subcarriers, arriving at a specific antenna is negligible, calculation of the ToF is also considered. ToF is used to calculate the complex exponential of the phase shift, which appears as a coefficient for each subcarrier in the new steering vector of M antennas making a new steering matrix with one row and L column (L: number of paths). To complete the modifications on the steering matrix and make ready for the application of the MUSIC algorithm, Spotfi implements another technique called CSI smoothing to get independent measurements. For this purpose, they first introduce the concepts of subarrays as a

portion of steering vector (considering the phase shift between antennas and the complex exponential phase shifts across subcarriers) and suggest a new structure made by multiplying and shifting the elements of the first subarray. They conclude that with the mentioned structure, MUSIC is applicable and consequently arrange the collected CSI with respect to the optimized structure to get the smoothed CSI. To detect the direct path, spotfi assumes the smallest ToF as its criteria and by assigning a likelihood function; it finds the path, which shows minimum variations between received packets. At the localization phase, Spotfi shows a median error of 0.4 m.

In reference [42] a fingerprinting-based method is proposed. The approach of PhaseFi is straightforward with minimum calculation complexity. It takes the raw CSI data received by three antennas over 30 frequency for 38 training points in the living room and 50 training points in the laboratory, applies a linear transform on the phase information, then feeds the processed phase data into a deep three hidden-layered neural network. Where a greedy algorithm is in charge of layer-by-layer training. This kind of training is adopted at the restricted Boltzmann machine (RBM) to tackle the phenomenon of vanishing gradient, a common problem in deep networks. When the weights and biases are tuned and the deep network is able to extract the important features of its input to reconstruct them at the output, the fingerprint database is ready and the system can perform the localization. One important point of PhaseFi is the application of the aforementioned linear transform on the raw phases of CSI data, otherwise referred to as phase sanitization. For this purpose, it defines the parameters that influence the phase such as measurement noise, time lag, unknown phase shift, and FFT size. The sanitized phase is obtained through a linear equation containing these parameters and the raw CSI phases. After sanitization, phases become concentrated into a small sector whereas raw phases are scattered and it is impossible to assign an angle to them. The localization phase takes advantage of a probabilistic approach based on Bayes law. Having the prior probability of a location in the fingerprint database, posterior probability finds the similarity between the inputs and the reconstructed outputs. The position of the target is calculated as the weighted average of all posterior probabilities. The mean error of PhaseFi is 1.08m in the living room and 2.01 in the laboratory.

Reference [43] suggests another fingerprinting-based method similar to PhaseFi, called DeepFi, which takes advantage of deep learning joint with a greedy algorithm at the training phase, and a probabilistic method at the localization phase. In DeepFi, CSI data, sent by an access point,

is collected from three antennas of a Dell laptop, in two different environments, the living room, and the laboratory, and 90 extracted amplitudes per location from all subcarriers, are fed into a deep neural network. The deep network comprises stacks of RBMs, where the greedy algorithm is in charge of layer-by-layer training to get optimal weights and biases to reconstruct the input data. Updating the weights at each iteration is done using contrastive divergence to reduce the time complexity. It also adopted a technique to tackle the complexity of computation and the need for less time of processing, in which the whole packets of CSI are divided into sub-groups of CSI packets called batches to be processed in parallel. The process of training comprises three steps, pre-training followed by unrolling and finally fine-tuning. In the stage of pre-training, four layers with decreasing order of neurons, reduce the dimension of the inputs. Weights and biases of each layer are separately calculated using the greedy algorithm and at the end of pre-training where the weights and biases are obtained, the downsized input at the output of the fourth layer goes under unrolling process to reconstruct the initial inputs by training layer five to eight with a probabilistic unsupervised approach. Finally, the reconstructed inputs are compared with the actual inputs to reduce the error of weights and biases at the fine-tuning phase. Then the weights and biases are stored in the fingerprint database. At the localization phase, the target sends a ping to the access points to request for CSI packets. The system applies the same process on the received CSI to reduce its dimension followed by reconstruction and fine-tuning. Finally, the system matches the weights and biases with the closest features in the fingerprint database to locate the target. DeepFi achieves approximately 0.95 m error for the living room and 1.8 m for the laboratory.

In reference [44] a device-free method called LiFS based on the model of power fading is presented by Wang et al. LinFS function relies on the fact that, in a multipath environment, fading phenomenon does not affect all subcarriers equally. Considering propagation, diffraction, and target absorption fading it defines a theoretical model of power fading and compares the actual signal power with the calculated value to decide which subcarriers behaviour comply with the model and calls them “clean sub-carriers”. In their model, they took free space propagation loss, the attenuation due to First Fresnel Zone (FFZ), and the measurement noise into account to “filter out dirty carriers” based on their actual CSI amplitude and the theoretical expected values, during the pre-processing phase. The whole experiment is conducted in a section of a library to benefit from its structure to have LoS and NLoS signal reception. In the positioning phase, the localization is done based on the relation between the pre-processed CSI and the locations of the target. Based

on the results presented in their work, LiFS localization error is under about 1.5m for 80% and 1m for 50% of estimations.

Reference [45] focuses on the direction of arrival (DoA) considering the azimuth and the elevation of the incident, as the important feature of the received signal to build up the fingerprint database. In their method, two phase-shifts are addressed the first one is produced by the structure of receiving antennas which are a uniform circular array (UCA) of omnidirectional antennas. The second phase shift is caused by the different time of flight (ToF) of CSI signal for 30 sub-carriers. Then it argues that the phase-shifts introduced in the CSI matrix report, otherwise called a steering matrix, can be considered in two directions: row-wise and column-wise phase-shifts. DoA causes phase shifts among rows and ToF results in phase shifts among columns. The steering matrix or manifold is composed of steering vectors related to each of the l signal paths. Every steering vector contains the phase shifts at the lth path resulted from different AoA and ToF of each incident of the kth subcarrier received at mth antenna. Next, it transforms the manifold from element space to beam space by multiplying it by the beamformer in order to get a virtual manifold with Vandermonde characteristics to make it ready for applying the SpotFi method. From this point on, their method is similar to SpotFi [30], in that, the rows of CSI matrix, which correspond to the number of antennas, are stacked in a column to form the steering vector as a single observation. Then, CSI smoothing is applied to extend the number of observations to make it ready for the MUSIC algorithm. Finally, the authors argue that smoothing decreases the Root Mean Square Error (RMSE) to less than one degree for DoA estimation.

Reference [46] addresses two disadvantages of previous researches. First, ignoring the CSI phase information because of the random phase shift disturbance. Second, the common metric of Euclidean distance otherwise known as log-likelihood, which should be minimized to map the test point with the point in the database. However, as the author says, considering this metric is correct only for small areas. It defines an effective coverage range (ECR), around 2cm when using the frequency equal to 2.4GHz. To tackle these two challenges it suggests considering the phase information after applying a novel phase sanitization method on it to reduce its random variations for the first issue, and as a solution for the second problem, it proposes a novel distance metric based on the AoA and two distinct measurements while moving toward the target. Experimental results of this work, show that their proposed phase sanitization method is more efficient in removing phase randomness resulted from other methods.

In reference [47], Wang et al, propose a fingerprinting-based method called CiFi. The main idea of CiFi is to collect 960 packets of CSIs per location, from three antennas, find the phase difference between antennas 1 and 2 as well as antennas 2 and 3 which makes 60 measures for each received packets of CSI. The reason why CiFi exploits the phase differences instead of the phases is the unstable nature of phases while the phase difference shows fewer variations. In the next step, CiFi calculates the AoA for each group of 60 phase differences and since there are 960 received packets, it divides them into 16 groups of 60 packets and calls them images. As a result, it constructs 16 images of 60 x 60 elements, where the number of rows or elements on the columns indicates 60 phase differences and the number of columns refers to 60 packets. Then these images are fed into a deep convolutional neural network (DCNN) at the training phase to train the weights. At the training phase, the feature map is extracted from the images by the convolutional layer followed by the subsampling layer, otherwise known as the pooling layer, which is in charge of resolution reduction of the feature map. Finally, a simple neural network works as the fully connected layer to perform the training. CiFi localizes its target using a probabilistic method. With the new collected CSI from an unknown location and the trained DCNN, the matrix of estimation is obtained. Then by applying a greedy method, the largest outputs are selected followed by a calculation of the weighted average of the selected outputs to localize the target. CiFi localization error is under 1 m for 40% of test locations.

Reference[48] presents another fingerprinting-based method similar to CiFi but it takes advantage of a convolutional neural network (CNN) and instead of phase differences it takes CSI amplitudes and constructs its CSI feature image. ConFi takes the amplitude of CSI data on each of the three antennas and maps the collected CSIs of each antenna to RGB channels of an image. As discussed in their research the resulted image for each point of reference is unique. It also argues that for CNN to avoid overfitting, the training data must be augmented. For this purpose, several techniques such as mirror, sliding window and choosing CSI samples in a random manner, have been used. It also gives a comparison between different sizes and the number of convolutional kernels in terms of accuracy. ConFi best result shows 1,36 m mean error of localization.

In reference [49], the adopted approach is based on the attenuation model to calculate the distance of the target from the AP. The authors opted for CSI instead of RSSI due to potential temporal instability of RSSI, which could lead to localization error. Moreover, since RSSI is a coarse-grained metric (i.e. only one measurement per communication) it cannot benefit from

advantages of CSI as a fine-grained metric (i.e. a package of information including communication links and multiple subcarriers) to address multipath related problems. Another advantage of CSI mentioned by the author is that CSI is from baseband, which exempts the system from further processing while for RSSI a down-conversion to the baseband is needed. In their experiment, the transmitters are three APs and the mobile laptop collects the CSI data at multiple RPs. Then a weighted averaging is applied on the 30 subcarriers to get the effective CSI. By doing so, the small scale fading effects are removed and the channel gain is considered from one single central subcarrier instead of 30 subcarriers. The next step is to find an appropriate indoor propagation model to express the relation between effective CSI and distance. For this purpose, a supervised algorithm takes the effective CSIs from two access points together with their known distances and trains itself to find the environment factor σ and the path loss exponent n. Then, using the obtained parameters and the effective CSI from the third AP, it evaluates itself on finding the distance of the third AP. Finally having the optimal parameters, the position of the mobile laptop is identified by using the triangulation method. It is argued that the proposed method shows temporal stability and its localization performance achieves an accuracy of 1.24 m error with a 0.57 m standard deviation.

Reference [50] suggests an improvement technique for DeepFi, termed as DNNFi, to reduce its computational complexity. In DeepFi there are N autoencoders for N reference points (RP) to be trained while the proposed method comprises a single supervised deep neural network (DNN) with four hidden layers and yet it achieves the same accuracy. As it is explained in DeepFi paper, each autoencoder is in charge of encoding and reconstructing the CSI features of a single RP without considering its coordinates and during this process, optimal weights and biases are obtained. However, in DNNFi coordinates are used as input labels hence the method is supervised. Similar to other fingerprinting (FP) methods, DNNFi includes two phases: offline and online. In the offline phase, two laptops are used as the AP and the receiver. The AP is at a fixed location while the receiver is placed on 31 RPs to collect the CSI data related to them, to normalize between 0 to 1, and to use them for training the system, and consequently obtain the optimal weights and biases. In the online phase, new CSI measurements from 9 unknown positions are fed to the trained system to find the probability of new CSI being related to RP in the fingerprinting database. DNNFi achieves faster computation with the same accuracy of DeepFi.

In reference [51] authors, propose a method, called MaLDIP with a quite similar main idea presented in LiFS, which removes the multipath affected subcarriers. MaLDIP is a device-free system, which detects the location of its target by finding the changes in received signal features due to the presence of the target in 15 uniform cells. The signal features at each location follow a temporal model but at the same time, due to the frequency-selective nature of the channel, they may be affected by multipath, which leads to different signal strength. Therefore, to assure a higher accuracy, it removes the subcarriers, which do not comply with the diffraction theory by adopting a threshold to choose optimal subcarriers. The whole experiment has two phases: offline and online. In the offline phase, CSI data is collected without the presence of the target person. Then CSI is gathered again with the human in every 15 cells. The fingerprinting database is build up by subtracting the two sets of collected CSI. As argued in their work, for best subcarriers one should expect a decrease in the amplitude of CSIs larger than the threshold, hence these subcarriers may be considered as conforming to the diffraction theory. After removing the undesired subcarriers, the matrix of the location's most important features is generated using PCA. At the localization phase, the collected CSI is preprocessed and normalized and the SVM is used to estimate the location of the target. MaLDIP achieves 93.6% accuracy in detecting the correct cell.

Reference [52] presents a method called modified matrix pencil (MMP) which improves the existing 2D-MUSIC presented in SpotFi, in terms of reducing its computational time. As we know from SpotFi paper, the 2D-MUSIC algorithm is based on finding a jointly estimated AoA and ToF related to peak values of MUSIC spectrum by taking advantage of super-resolution algorithm. The authors of MMP claime that their method reduces the computational costs of SpotFi to around 200 times faster, while achieving the same accuracy. MMP method is based on replacing 2D-MUSIC with 2D matrix pencil algorithm where instead of 2D estimation, AoA ans Tof are estimated separately. The CSI is collected on three receiving antennas then the enhanced CSI matrix is constructed next by applying some mathematical modifications such as singular value decomposition, Eigen decomposition and permutation of AoA and ToF are calculated. MMP proves to be 203 times faster than 2D-MUSIC with signal to noise ratio (SNR) of 35 dB and 196 times faster when there is no noise.

Reference [53] introduces another device-free otherwise called a passive method, which uses the amplitudes of CSI information without any previous feature extraction to construct the related image labeled by the coordinates of each location using a six-layer CNN-based deep learning

scheme for image recognition with a classification approach. The data collection process is done using two laptops placed at fixed locations with the device-free target at 22 different points in the office and 25 points in the corridor, and hundred measurements per location under 5.32GHz band. The presence of target at each location has its unique effect on the characteristics of the received CSI data and collected information is arranged to three matrices of 30x30 size representing the channels of RGB image for each location. At the training phase, the constructed images (65 for the office and 40 for the corridor) are fed into CNN where four layers are in charge of feature extraction and two fully connected layers perform the classification. At the test phase, 10 images for the corridor and 15 images for the office are used and the reported average localization error for PILC is 1.843 m.

One important issue in localization is the computational burden and complexity. In reference [54], a "model-free" approach is presented by implementing a technique based on continuous logistic regression and relying on a deep learning system to score an accuracy of 97.2 cm. The idea behind this method, as suggested by the authors, is to replace the traditional method of training and localizing in two phases with a system capable of modeling the signal features with regard to the location. The other aspect of their work is the "unified optimization framework" in which the relation between collected CSIs and the correspondent locations is formed to present a system of optimization for localization systems by minimizing the mean distance error between the predicted and true locations. The proposed method also benefits from a technique to assure less randomness during the training processing since small perturbations are introduced during the training phase. In the data collection, phase CSI data is collected in two different environments: laboratory and corridor. In total, 60000 packets are collected and after phase extraction, calibration, and data augmentation by perturbation distance, the resulted processed data is fed into MLP and CNN.

Reference [55] addresses the insufficient number of access points in some locations and in order to solve the problem, it suggests a new method of fingerprinting with only one AP. As the raw phase is not an appropriate metric for fingerprinting, authors introduce a method comprising outlier removal, phase sanitation (reducing the effects of carrier frequency offset CFO due to unsynchronized Tx and Rx, and sampling frequency offset SFO due to unsynchronized clocks of ADC), and phase decomposition to get the phase information of multipath followed by dimensionality reduction using PCA and feature extraction to build up the fingerprinting database. The experiment is done in three different places, laboratory, meeting room, and corridor,

considering two experimental scenarios related to the mobility (number of people): static and dynamic. Moreover, experimental environments are divided into cells with an identifying number where 1000 packets at the training phase and 200 packets at the estimation phase are collected. The efficiency of the proposed system is evaluated by KNN and SVM as deterministic, and Bayes as probabilistic algorithms. Finally, a comparison by RSSI-based and CSI-based systems is given. According to their results, SVM proves to be more efficient among three matching algorithms by the accuracy of 0.6 m and 0.45 m in the laboratory and the meeting room, respectively. Also, having multiple decomposition paths does not lead to higher accuracy while 2-3 and 4-5 of them are the optimal number depending on the environments.

One of the most recent researches on localization using CSI is presented in reference [56]. The authors introduced a device-free method using the amplitudes of CSI and RSS to localize a person using a router with two antennas as the transmitter and a personal PC equipped with Intel 5300 network interface card with three antennas as the receiver, both at fixed places. During the training phase, a person stands in 16 locations and the transmitter starts the communication with the receiver. These 16 points form 16 different classes so the localization is addressed as a classification problem. The receiver collects 15 packets of CSI and the RSS values are available on three receiving antennas for each location. Fifteen packets are concatenated to consider environmental changes. Moreover, three persons with different body types have participated in the experiment to assure the robustness of the system. The collected CSI and RSS data are processed using specific data fed into two different neural networks, MLP and 1-D CNN. Authors argue that choosing 1-D CNN reduces the network complexity and the overhead of conversion caused by 2-D CNN, which leads to a less computational burden. As the research, results show 1-D CNN outperforms the MLP network by maximum localization error of 0.92m with the probability of 99.97% compared to 0.92m of localization error with 81.07%.

CHAPTER 3 ARTIFICIAL NEURAL NETWORK

3.1. Introduction

In this chapter, we will explore the general concept of artificial neural network (ANN), two ANN structures which are used in this experiment, and the applications of in regression and classification.

3.2. The definition of an Artificial Neural Network

An ANN; invented by Robert Hecht-Nielson; can be simply defined as a processing system composed of a number of interconnected units, known as neurons, arranged in multiple layers containing activation function to imitate the functionality of a human brain in order to process the information and learn to model the behaviour of an unknown system.

3.3. Applications of ANN

ANN is generally capable of two main tasks namely modeling a linear or non-linear relation between input and output data of a complex system, and classification of input data without having any target data. The first one falls into the supervised learning method category and the latter is an unsupervised learning algorithm. The goal of using ANN for modeling a system is to be able to estimate the output of the system for unknown inputs as long as the training data is rich enough to provide a decent knowledge of the unknown system. On the other hand, using an ANN as a classifier is interested when we want to find out to which category our input data belong.

3.4. The general structure of an ANN

A basic mathematical representation of a single artificial neuron can be seen in [fig.3.1] and [Eq.3.1]. As it can be seen, all inputs are multiplied by the appropriate weight and the sum of all weighted inputs with bias goes through the activation function to generate the output y, which could be an estimation of a desired target or a value representing a class of inputs. In practice, multiple neurons are needed and depending on the necessary depth of the network, hidden layers are added.

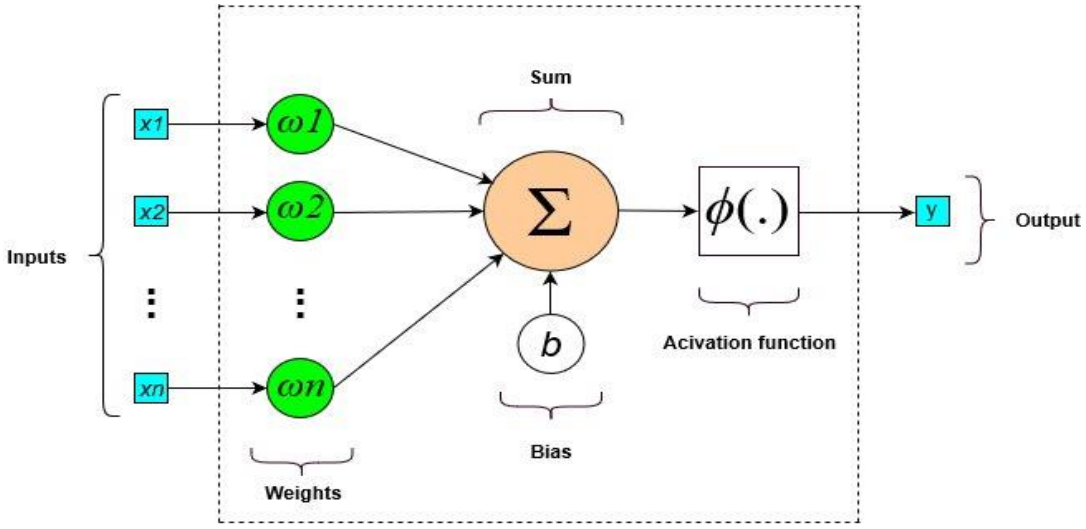

Figure 3. 1 Mathematical representation of an artificial neuron

$$y = \phi\left(\sum_{i=1}^{n}(x_i \cdot \omega_i) + b\right) \tag{3.1}$$

In [fig3.2] a simple ANN with two hidden layers and two outputs is presented. Each green circle is in fact the combination of weight, bias, and the activation function.

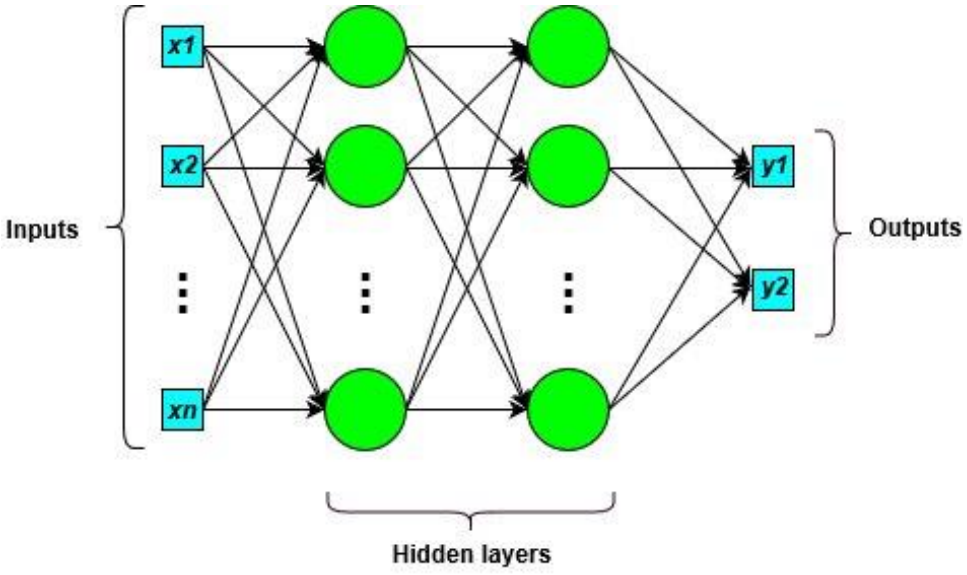

Figure 3. 2 A simple multilayer ANN

3.5. Activation functions

As mentioned, a neuron needs an activation function to generate its output. There mainly two groups of activation functions namely traditional and modern functions. Each function has its specific properties and its appropriate for a specific application. An overview of two groups of activation functions is presented in [fig.3.3]. Among the presented functions, Sigmoid, Hyperbolic tangent, and Relu are the most popular functions [61].

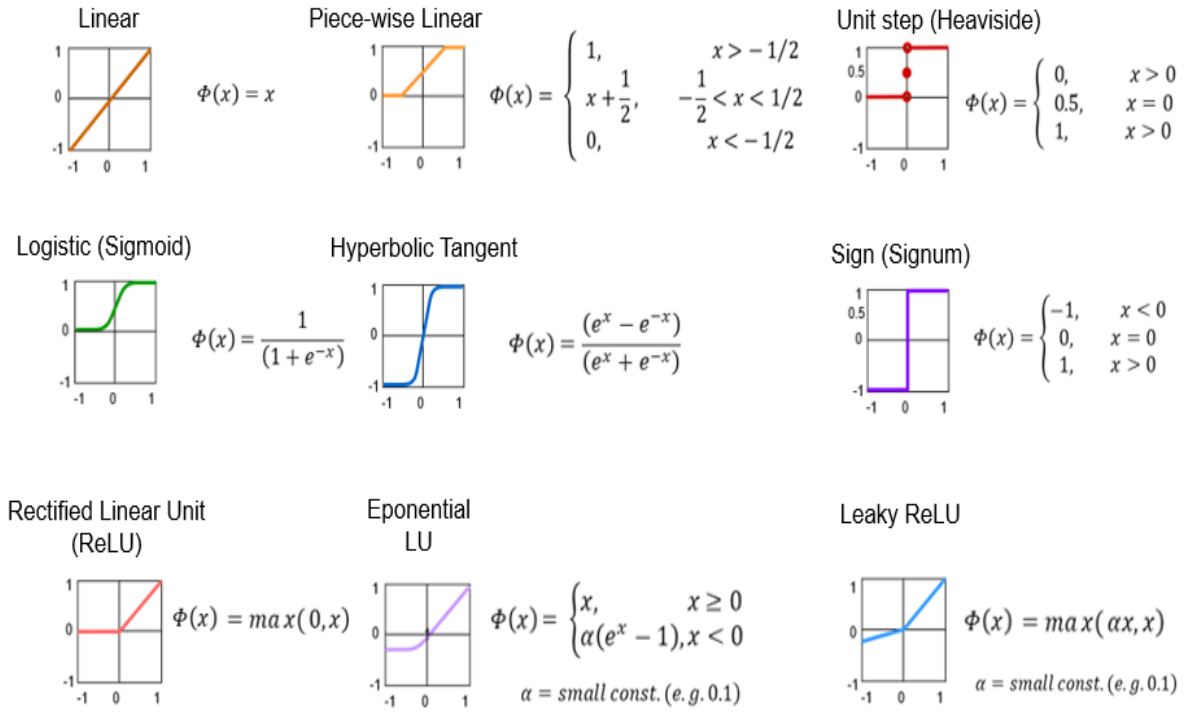

Figure 3. 3 Different types of activation functions

The activation functions are used to consider the non-linear nature of data in real life data. The input of activation function is the weighted sum of previous layer's output plus bias on which a mathematical operation is performed. The role of bias is to shift the shift the activation function to a desired direction for the model to fit best for our set of data.

3.6. Different types of ANN

ANNs are generally categorized in three groups of feed forward, feedback otherwise known as recurrent, and convolutional neural networks.

3.6.1. Feedforward ANN

Figure 3.2 shows a feedforward ANN (FFN) in which, the flow of data is uniquely from input toward output to associate inputs wit outputs, and there is no feedback loop. Then at the output layer, the estimated target is calculated and considering the chosen loss function, usually Mean Squared Error (MSE) [Eq.3.2], the error between actual and estimated values is estimated and its gradient is back propagated to the network to update weights and biases for the next iteration.

$$MSE=\frac{1}{n}\sum_{k=0}^{n}(Y_k-\hat{Y}_k)^2 \tag{3.2}$$

Feedforward ANN can be sub-categorized in one-layer, shallow, and deep (3 or more layers) network. Choosing the appropriate ANN depends on the complexity of the relation between input and target data. As a common application of FFN, object recognition can be mentioned. The main application of FF networks is mapping, in other words, to model the relation between inputs and targets.

3.6.2. Recurrent ANN

Despite the one-way flow of data in feedforward ANN, in a recurrent ANN there are feedback connections from a layer to the previous layer or from a neuron to itself [fig.3.4], which give RNN a sort of memory and a dynamic behaviour and enable it to solve problems that are more complicated. RNN constantly changes its state to be trained and when it is fully trained on a given data, it reaches its equilibrium point. RNNs are mostly used for sequential tasks such as time series problems.

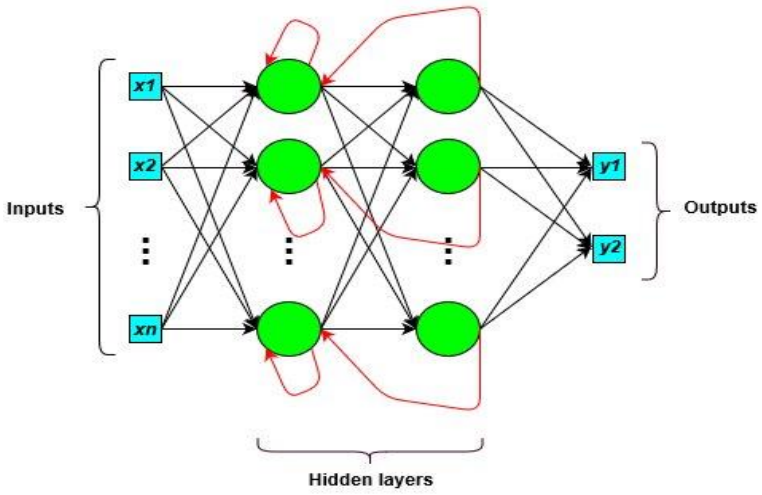

Figure 3. 4 Recurrent Neural Network

Natural language processing is a well-known application of RNN. The limitation of RNN is its short-term memory, so Long Short-term Memory networks (LSTM) are proposed to solve the problem.

3.6.3. Convolutional ANN

This type of ANN is popular; due to its three-dimensional architecture; for applications in computer vision such as self-driving cars. As it can be seen in fig.3.5, the first layer is convolutional layer followed by pooling layer and so on.

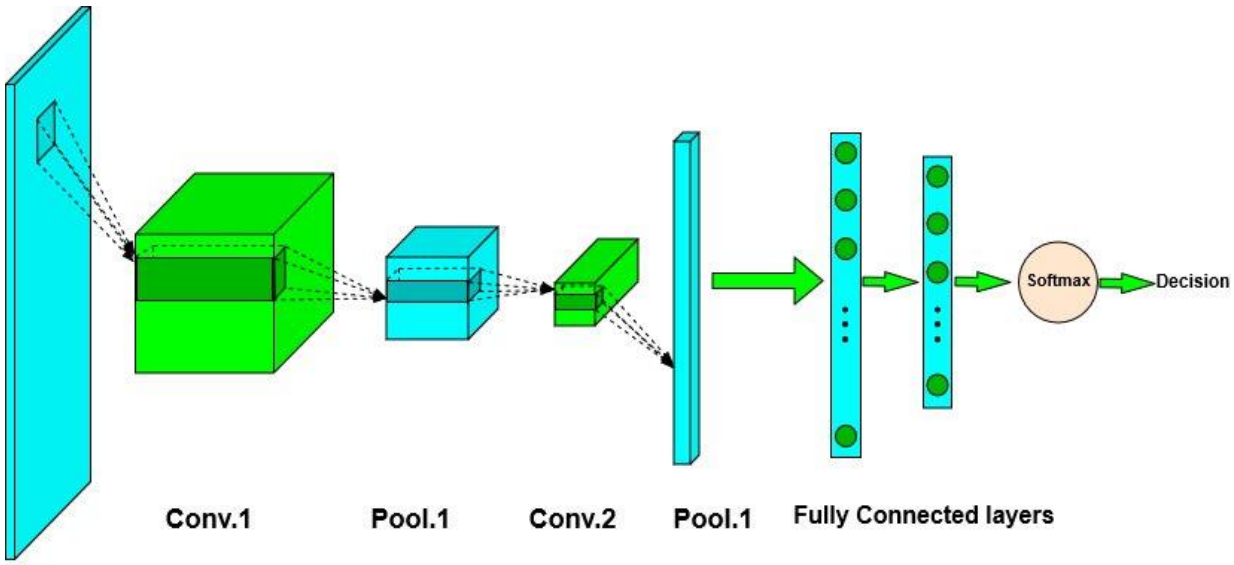

Figure 3. 5 Convolutional Neural Network

The task of convolutional layer is to detect pattern such as edges, corners, circles, shapes, and texture. For this purpose this layer slides a filter, technically a matrix of m*n for which the values are initialized with random numbers, across all sets of input data of m*n size and to calculate the sum of element wise product of the filter and the set of pixel matrices [fig.3.5]. The challenge is the size of the filter and the effect it has on the output size comparing the initial size of input data. If a filter of f*f size slides over an image of n*n size to perform convolution, the output size will be (n-f+1) * (n-f+1). Which means the input shrinks, to overcome the problem zero padding is used which in fact is a border of zeros around the input.

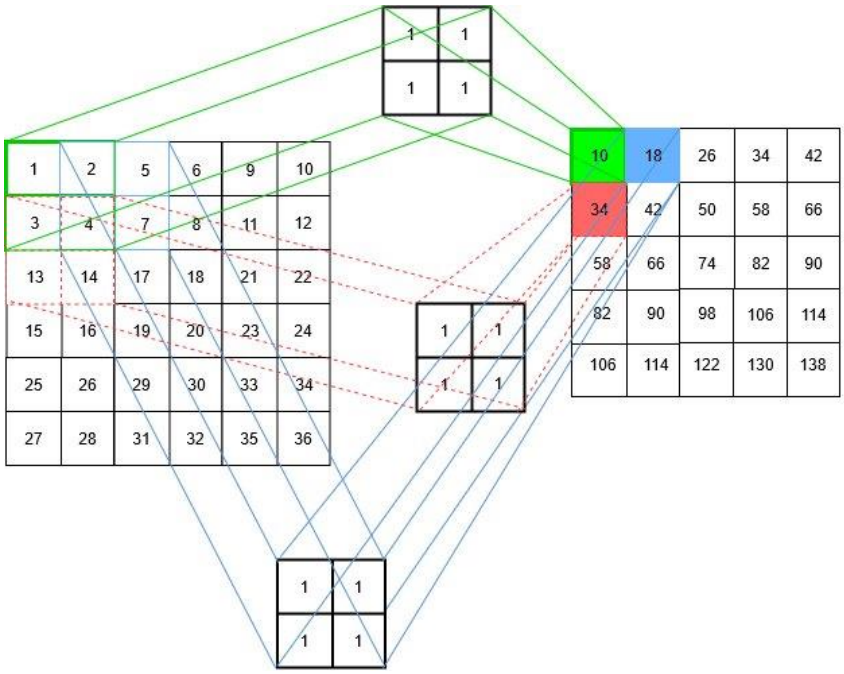

Figure 3. 6 An illustration of convolution operation

In the next layer, max pooling is done by applying an n*n filter to reduce the dimensionality by reducing the number of pixels in the output of previous convolutional layer. This filter finds the maximum value among all values that are scanned at each max operation and subsamples the data. Another parameter is the stride, which defines the number of pixels the filter move as it slides across the input data. To get an insight into the functionality of max pooling let us consider n=two and the stride =two. At each max operation, the filter finds the maximum of 4 values in the input data, then it moves two pixel to the right and performs the same operation. When all input data are processed, the size of resulted matrix is half the size of original matrix.

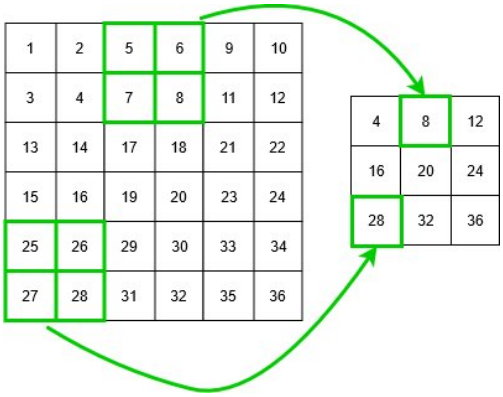

Figure 3. 7 Max pooling

3.7. Different methods of learning

There are three learning methods for training an ANN namely supervised, unsupervised, and reinforcement learning.

In supervised learning, we have a set of data containing inputs and outputs. The ANN begins with random values and estimates the target. The estimated value is compared with the actual target and the error is sent back to correct the weights and biases hence the name supervised.

Despite supervised learning, unsupervised learning has no actual target so the network finds the similarities among the input data and categorizes them into classes. In fact this kind of network works on its own and does not need a supervision, hence the name unsupervised.

Third group of learning is working somehow in between two previous groups. In RNN, we have a policy network [fig.3.8], which is in charge of collecting experiences by transforming inputs to output actions, using policy gradient.

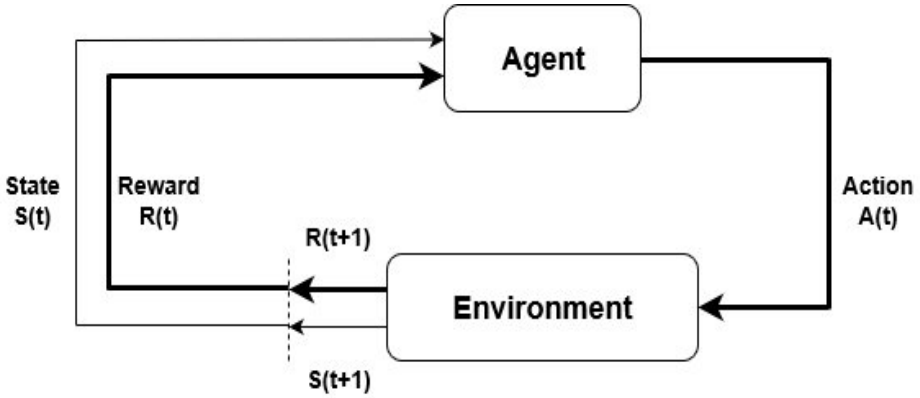

Figure 3. 8 Policy Network

To get an insight into the functionality of RNN, let us explain with an example. Assuming our net network is about to learn the pong [fig.3.9] playing with a professional pong player. The agent starts with a random state and waits for the scoreboard results. If it scores a goal, it will receive a reward of +1 and in case the professional player scores a goal a reward of +1 will be assigned to the agent. Each reward of +1 leads to increasing the probability of that action in the future. The ultimate goal for the agent is to try multiple actions with different directions considering the previous ones and the related rewards to optimize the policy to receive as much of

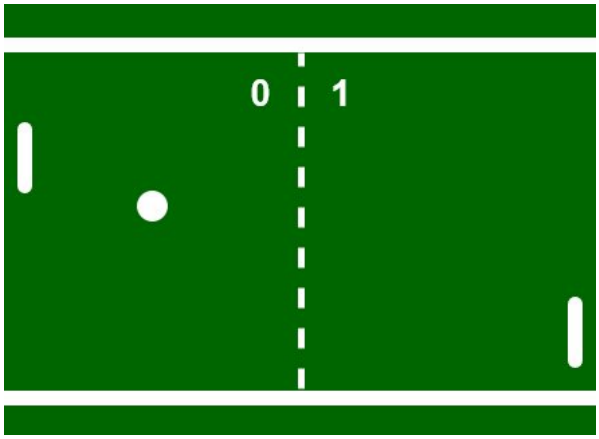

Figure 3. 9 The pong game

rewards as possible. On the other hand, -1 leads to filtering out the bad actions and they will be less likely to happen in the future.

3.8. Overfitting and under fitting

Overfitting takes place when the ANN is trained to learn all the details of a given input data including the environment noise and the temporary changes in the behaviour of the unknown system. Obviously, this ANN will perform perfectly using the data on which it is trained however, since noises and changes in input data are not constant, the performance of ANN will significantly drop with a new set of data. On the other hand, when the ANN ignores many details about the input data, it will not be capable of knowing the nature of the unknown system. An under fitted ANN cannot find the patterns in the input data and will show a poor performance. Figure 3.10 illustrates an over fitted, under fitted and a fitted ANN.

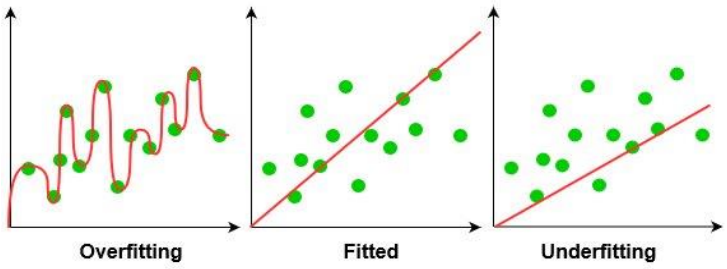

Figure 3. 10 An illustration of an over fitted, under fitted and a fitted ANN

To overcome the overfitting there are techniques such as increasing the number of finding the optimized number of layers and the neurons in each layer, input data, using validation set, decreasing the number of iterations, and cross validation. To solve the problem of under fitting logically system needs more time by increasing the number of iteration and reliable data for training. In addition, changing the number of layers and neurons and activation functions may solve the problem.

3.9. MLP and GRNN

In our experiment, we use MLP and GRNN to perform the regression. [Fig.3.11, 3.12] depict the abstract structure of an MLP and a GRNN network. We use Multilayer Perceptron (MLP) with one and two layers, and General Regression Neural Network (GRNN) with two different spread factor to get the minimum localization error.

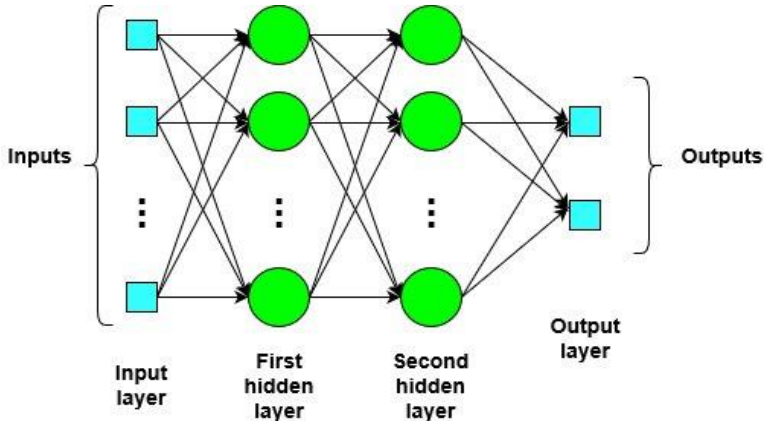

Figure 3. 11 The general structure of an MLP network with two hidden layers

The decision about the number of layers and the spread factor is based on trial and error. We realized that the performance of an ANN with more than 2 layer drops compared to ANN with two layers.

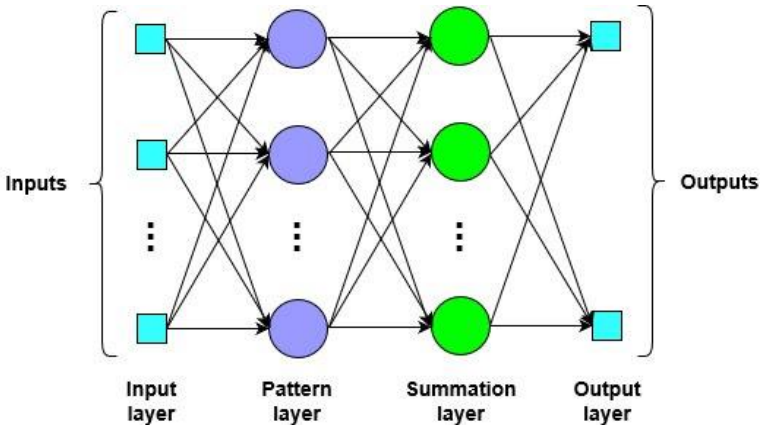

Figure 3. 12 The general structure of a GRNN network

MLP is a feedforward ANN with at least three layers namely input, hidden layer/s and output. Each node in each layer is connected to all neurons of previous and next layers hence MLP is a fully connected ANN. The process of learning begins with assigning random values to weights and biases. Then the network takes the inputs, multiplies them to the initial weights, adds biases, calculates the sum and passes it through the activation function to obtain the estimated output to compares it to the actual value for error calculation. The calculated error is back propagated to the network using gradient descent to minimize the estimation error by updating the weights and biases at each iteration.

MLP is good at distinguishing non-linearly separable data; hence, it can be used for nonlinear regression by mapping the known measures to their relevant coordinates. In our experiment, we tried various configuration with regard to the number of hidden layers, the number of neurons in each layer, and the activation function of each layer. More hidden layers do not lead to better accuracy but the performance of a complicated network is poor with regard to the localization error.

On the other hand, generalized regression neural network (GRNN) which is a variation of radial basis neural networks, uses a one-pass procedure with no back propagation as its training algorithm and no training parameters as in MLP. GRNN as a supervised network performs function approximation between given input and output data, directly and quickly using the training data. GRNN as an associative memory memorizes every specific pattern when the one-pass training is done. Consequently, the memorized patterns are generalized to new set of data to generate the

output. The function of GRNN is based on estimation of most probable output value for a given input by computing the joint probability density function of inputs and outputs.

Similar to MLP, GRNN can be employed for regression and classification. The structure of GRNN consists of input, pattern also known as hidden (with Gaussian activation function), summation, and output (division) layers. The input layer takes the training set and feeds it to the pattern layer, where the Euclidean distance is calculated. For each pattern in the training set there is a neuron in the pattern layer although too many pattern in the training set could lead to poor functionality of GRNN. The summation layer consists of two types of neurons namely the Numerator or summation neurons (equal to the number of outputs) and Denominator or a single division neuron. The training set is multiplied by the activation function and summation presented at the Numerator neurons. The division or the Denominator neuron is in charge of summing the activations function. The output layer divides the received signal from summation (Numerator) neuron by the signal from the division neuron (Denominator). Eq.3.3 shows the predicted value using Parzen's non-parametric estimator at the output layer of GRNN.

$$Y(x) = \frac{\sum_{k=1}^{N} y_k K(x,x_k)}{\sum_{k=1}^{N} K(x,x_k)} \tag{3.3}$$

$$K(x, x_k) = e^{\frac{D_k^2}{2\sigma^2}} \tag{3.4}$$

$$D_k^2 = -(x - x_k)^T (x - x_k) \tag{3.5}$$

Where N is the number of observations. σ the spread/smoothing factor is the width of sample probability or the size of the neuron's region. $Y(x)$ represents the prediction value of input, y_k the activation weight for the pattern layer neuron at k, and $K(x, x_k)$ is the Radial basis function kernel (Gaussian kernel Eq.3.4) and D_k^2 shows the squared distance between the input vector *x* and the training vector x_k. Small value of σ leads to non-Gaussian shapes, while larger value of σ smooths the estimated density, and finally forces it to become a multivariate Gaussian with covariance of unity. To find the optimum spread factor, a range of values must be tried empirically. In our experiment, the optimal values of spread factor for each of two scenario are determined by multiple observations and comparison between results. Although having only one parameter to set may seem an advantage for GRNN, in practice, the results from GRNN are not as good as that of MLP although, GRNN function is better at learning phase.

CHAPTER 4 CSI GEOLOCATION

4.1. Introduction

In this chapter, the background knowledge about CSI is presented, and then the geolocation method that is used in this research is explained in detail including the hardware setup, site surveying, training of the system, and the test phase [fig.4.1]. Experimental results are presented to approve the functionality of our approach.

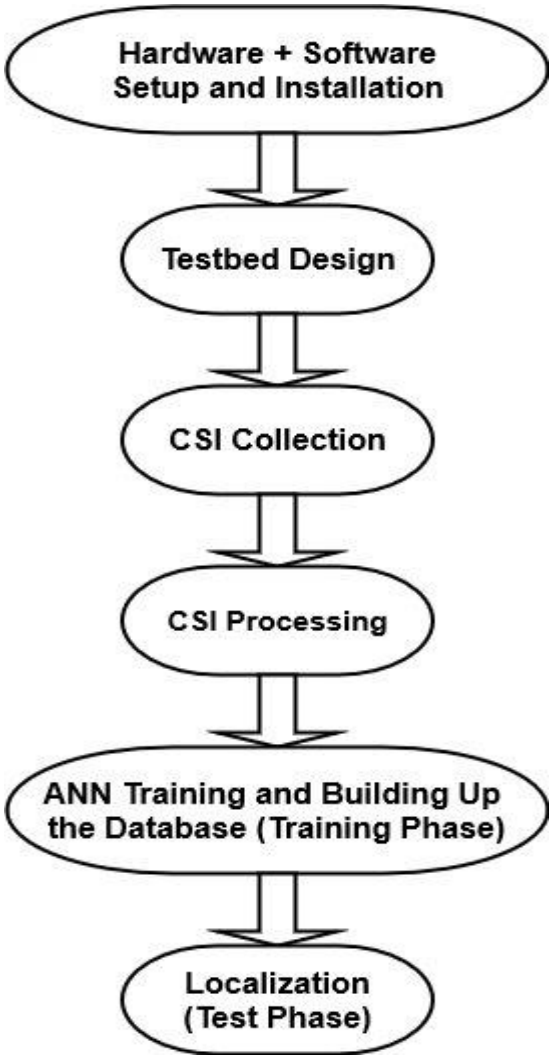

Figure 4. 1 The Flowchart of the experiment

4.2. Channel State Information (CSI)

The received signal maybe affected by its own multiple replicas at the receiver, which may constructively/deconstructively affect it. Moreover, fading and path-loss also, could affect the CSI packet. All these can be represented in CSI, which is an important information from the physical layer. Since we are using three transmitter and three receiver antennas, the communication is MIMO-OFDM, and considering 30 subcarriers the CSI report is a three dimensional matrix. Each CSI is a complex value referring to amplitude attenuation and phase shift of the received signal. It is essentially the channel frequency response (CFR), sampled at known frequencies. Therefore, to have a better understanding of CSI, one needs to have a clear idea about CFR. CFR is in fact, the channel impulse response (CIR), but in the frequency domain. The impulse response function of the communication channel demonstrates how the channel affects each different path in terms of its amplitude, phase, and delay due to fading, scattering, and power loss. To obtain CFR, a fast Fourier transform (FFT) should be applied to CIR. Equations (4.1) and (4.2) represent the CIR and CFR respectively [57, 58].

$$CIR = h(\tau) = \sum_{i=1}^{N} \alpha_i \, e^{-j\theta_i} \delta(\tau - \tau_i) \tag{4.1}$$

$$CFR = H(\omega) = FFT[h(\tau)] = \sum_{i=1}^{N} \alpha_i \, e^{-j(\omega\tau_i + \theta_i)} \tag{4.2}$$

Where α_i, θ_i, τ_i, and N represent amplitude, phase, delay for each signal on *i*th path, and number of total paths respectively.

As mentioned above, CSI is a series of H (ω) at k specific frequency and it can be demonstrated as a complex number as in equation (4.3):

$$\text{CSI} = \text{H}(f_k) = |\text{H}(f_k)| e^{j\angle \text{H}(f_k)} \tag{4.3}$$

CSI is included as a packet of complex values in the feedback, from the receiver to the transmitter to adjust the transmission parameters of beamforming in order to improve the functionality of the communication channel. According to table 7-25f in IEEE Standard reference [5], the size of the CSI report depends on the bandwidth and the number of carrier grouping as shown in [Table 4.1]. N_g refers to the number of adjacent subcarriers represented by a single subcarrier.

The provided CSI report by IWL5300 is in a specific format where 30 subcarrier groups are reported as the channel matrices. Now, if the bandwidth 20 MHz is selected, each of these 30

subcarriers represents two consecutive subcarrier of OFDM hence N_g is 2. $N_g = 2$ means every two adjacent subcarriers are represented by one, so we see that subcarrier indices begin from -28 which means two subcarriers -28 and -27 are represented by a single subcarrier -28 or -26 is the representative subcarrier for -26 and -25, and so on. Hence, if we choose Ng = 2, the total number of subcarriers for which the matrix of CSI is sent, becomes 30.

Table 4. 1. Number of matrices and carriers grouping [5]

BW	**Grouping** N_g	***Ns***	**Carriers for which matrices are sent**
20 MHz	1	56	All data and pilot carriers: -28, -27,…-2, -1, 1, 2, …27, 28
	2	30	-28, -26, -24, -22, -20, -18, -16, -14, -12, -10, -8, -6, -4, -2, -1, 1, 3, 5, 7, 9, 11, 13, 15, 17, 19, 21, 23, 25, 27, 28
	4	16	-28, -24, -20, -16, -12, -8, -4, -1, 1, 5, 9, 13, 17, 21, 25, 28
40 MHz	1	114	All data and pilot carriers: -58, -57, …, -3, -2, 2, 3, …,57 ,58
	2	58	-58, -56, 54, -52, -50, -48, -46, -44, -42, -40, -38, -36, -34, -32, -30, -28, -26, -24, -22, -20, -18, -16, -14, -12, -10, -8, -6, -4, -2, 2, 4, 6, 8, 10, 12, 14, 16, 18, 20, 22, 24, 26, 28, 30, 32, 34, 36, 38, 40, 42, 44, 46, 48, 50, 52, 54, 56, 58
	4	30	-58, -54, -50, -46, -42, -38, -34, -30, -26, -22, -18, -14, -10, -6, -2, 2, 6, 10, 14, 18, 22, 26, 30, 34, 38, 42, 46, 50, 54, 58

The modulation and coding scheme (MCS) used for sending Frames of CSI is MCS 19, which means 16 QAM with coding rate of ½ for three streams sent from three antennas. In this experiment, we use 20 MHz bandwidth and 64-point FFT sampling with the number of carrier grouping of two. Therefore, we have 52 data, 4 pilot, and 8 null OFDM subcarriers with 312.5 KHz of subcarrier frequency spacing.

Moreover, all three antennas of transmitter and receiver are involved and for each measurement, 20 packets are sent. Therefore, the CSI report contains 20 structure of 3x3x30 signed 8-bit resolution complex values. Compared to RSSI as single value information, also known as coarse-grained, it is obvious that CSI contains detailed information, hence known as fine-grained. In other words, for each measurement, CSI gives comprehensive information related to how the communication channel affects each subcarrier in terms of phase-shift and amplitude attenuation.

Moreover, by using three antennas at both the communication channel ends, we can benefit from spatial diversity.

Thanks to this richness, CSI is not only less affected by temporal instability, but also, shows uniqueness for each measuring point. Fig 4.2 shows the uniqueness of CSI data for each location. Each color refers to variations of CSI amplitude over 30 subcarriers for a location at which, 20 packets of CSI are received. As can be seen, all received packets at a specific location show similar behavior and obviously different from that of other locations.

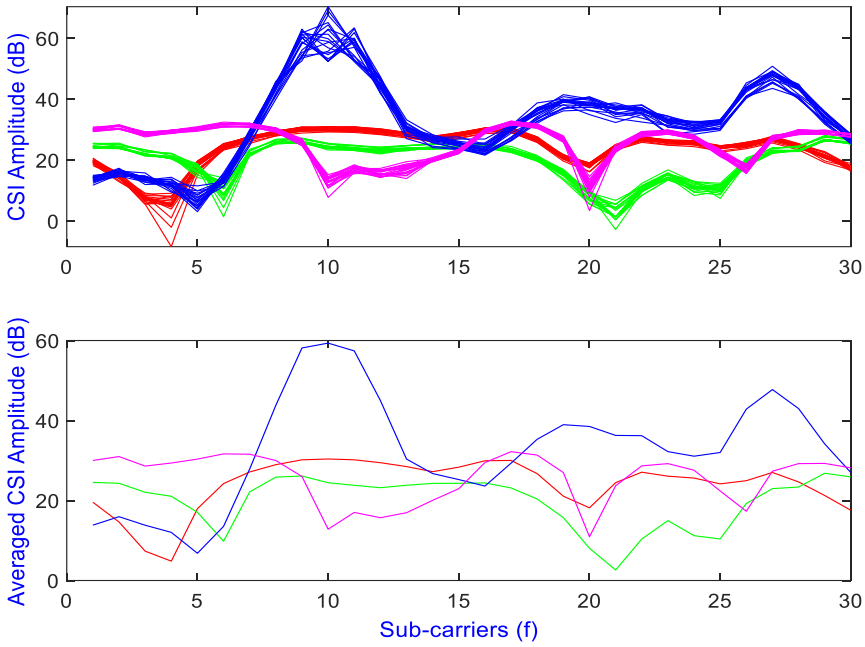

Figure 4. 2 CSI Amplitude of communication link 1(Tx1-Rx1)

For 20 packets and the average of them, at four measurement points

4.3. Hardware Installation and Setup

For our experiment, we use two Lenovo laptops equipped with Intel Wi-Fi Link (IWL) 5300 NIC network adaptor with three antennas [fig 4.2]. These three antennas give rise to nine wireless links between the AP and the MS. In addition, to get a coverage with longer range, we choose the operation band of 2.4 GHz so that the signal wavelength is around 12.5 centimeters. Moreover, the operating mode for this connection is set to “Monitor mode” in which the packets are sent and received at a fixed hardcoded address 00:16:ea:12:34:56.

In this research, all nine links between Tx1-3 and Rx1-3 are considered to exploit the spatial diversity. The reason for using this specific network adaptor is to have access to CSI data by installing a modified driver created by Daniel Halperin [1]. This modified firmware changes the previous Kernel on Linux Ubuntu operating system to a customized version. This customized kernel enables the debug mode of the network adaptor, and consequently at each communication session between two machines, a CSI report containing adjustable number of packets for 30 subcarrier groups (one group for every 2 subcarriers at 20 MHz) is received at the receiver machine upon the request sent by the receiver. The ensemble of obtained CSIs represent the unique and time-independent behaviour for each location. This data constitutes the appropriate signature for the fingerprinting technique.

To prepare our laptops, first Ubuntu 14.04.5 LTS 32-bit, with kernel 3.13.0-17 is installed on both machines. Then by running the installation instructions, presented at reference [60], in Ubuntu terminal, the modified kernel is downloaded and installed. The complete set of commands are given in Appendix A.

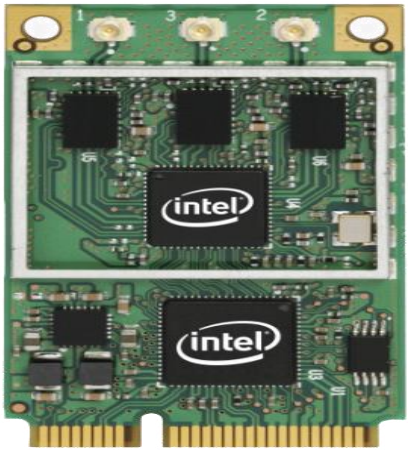

Figure 4. 3 Intel Wi-Fi Link 5300

The first laptop, which is considered as the transmitter (Tx), set in “injection mode”, is located at a fixed location on the sixth floor of the Lassonde building of Polytechnique Montreal. The second laptop considered as the receiver (Rx), set in “monitor mode”, is moved all over 200 distinct points of measurement. The distances between measurement points is set to 55cm resolution along the Y-axis and 110 cm along the X-axis. For each location, Rx sends a request to Tx, and in response, Tx sends back 20 WiFi packets of information across 30 subcarriers. [Fig.4.4, 4.5] shows the packet send and receive process between Tx and Rx. The receiver collects CSI data for data frames, which are identified by the same MAC address in the header for the source and

the destination as 00:16:ea:12:34:56 and the length of payload. Table.1 shows the set of subcarriers specified by IEEE 802.11n-2009 standard. Intel NIC 5300 supports measuring 30 OFDM subcarriers corresponding to Ng = two for 20 MHz. These subcarrier indices are used to determine frequency sampling in order to extract the relevant parameters from the received CSI. This operation bandwidth results in 50 ns of time resolution, which in turn is equal to having all the paths, which are shorter than 15 m in the same time bin.

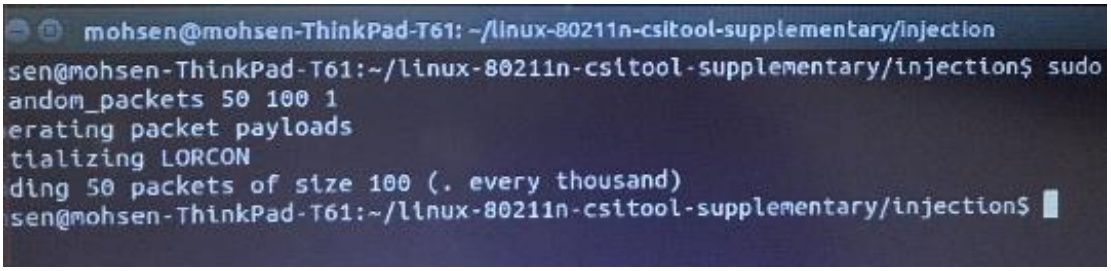

Figure 4. 4 Sending 50 packets from Tx

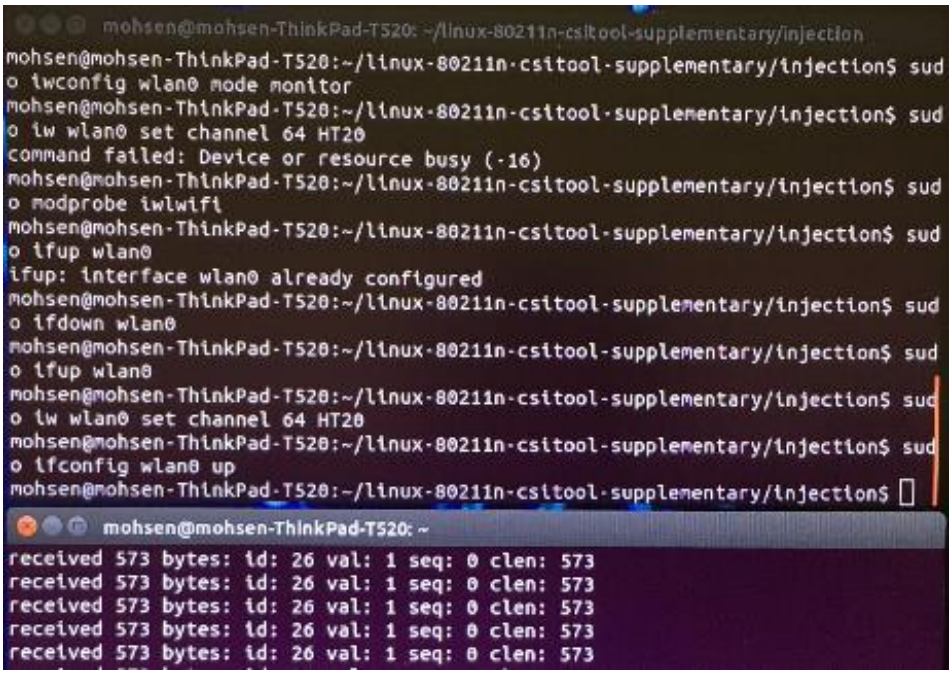

Figure 4. 5 Receiving packets on Rx

Once the CSIs are collected and processed for all locations, we use them with their associated locations to create the database at the training phase. Then, at the localization phase, the specific

measured signature is used as the input of the ANN, acting as the pattern matching algorithm, to locate the user's location.

4.4. Practical implementation

The ultimate goal of this experiment is to localize people in a building. Although we perform all steps of our measurement and localization on two Lenovo laptops, it is obvious that carrying a laptop, due to the size and weight, is not feasible. Therefore, the alternative solution for a real life scenario is to use an Intel NUC mini PC [fig.4.5] as it is used in Spotfi [30],

Figure 4. 6 Intel NUC mini PC, equipped with NIC 5300, presented in [30].

This mini PC together with the NIC 5300 can be attached to a person's belt so the height from the ground would be around 0.9 meter. Considering this fact, we place our target laptop on a flat shelf cart with the height of 0.9 meter to simulate the approximate real life scenario and for the ease of replacement as well.

4.5. Testbed design

For our testbed, we consider the sixth floor of Lassond building at the cafeteria. 280 points of measurement with 55 centimeter in y direction and 110 centimeter in x direction and all at the same height of 90 centimeter are chosen. The reason for the spacing between measurement points is the structure of cafeteria and the positions of the tables. The measurement campaign is done in

different days of the week at various times to find out if time may affect the CSI behaviour, and since CSI is less time variant than RSSI, no considerable change is seen.

During the measurement, the transmitter is at a fixed location and the receiver goes over 280 locations to record the CSI data. Measurement locations are chosen in a way to satisfy both line of sight (LoS) and non-line of sight (NLoS) communication between Tx and Rx [fig.4.6]. There is no direct path between the Tx and the measurement points located in the corridor and all that these points receive from Tx, is the reflection of the original signal and all points in the corridor are located in NLoS.

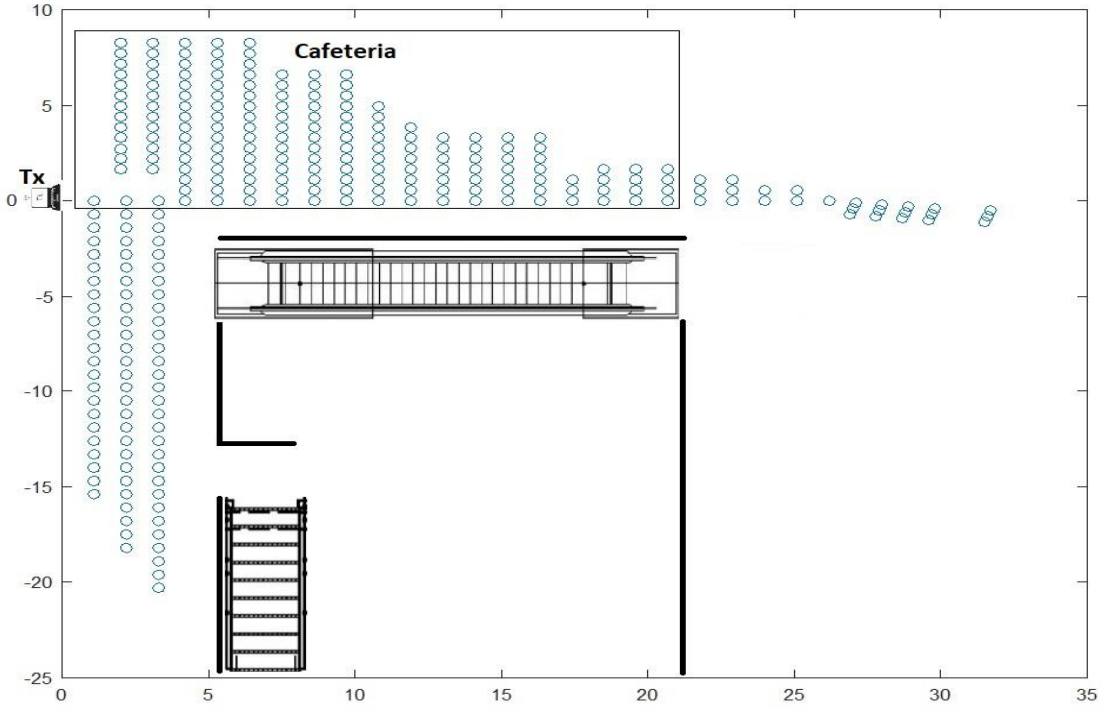

Figure 4. 7 Part of 6th floor including the cafeteria and the corridor

4.6. Offline Phase

The offline phase comprises three steps, namely collecting the fingerprint data, processing the collected data, and training neural network with the processed data. During the offline phase, ANN learns the relation of between CSI data and its corresponding coordinates for 80% of collected data. At the test phase, it estimates the coordinates of 20% of locations, which are unknown to it.

4.6.1. CSI Collection

In order to collect CSI data, the receiver is placed in monitor mode by running the appropriate code for receiver in terminal, and it waits until the transmitter starts sending the report. To set the number of packets, the delay between packets and the size of packets for each communication, the desired setting is applied by running the appropriate code for the transmitter in the Ubuntu terminal. The aforementioned codes are provided in Appendix A. During the measurement campaign, the mobile laptop's lid is always at vertical position.

4.6.2. Challenges for CSI preparation

Once the CSI report is received by the receiver, it is stored in a binary format. Considering a reference point as the origin with the coordinates (0, 0), a location number is given to each measurement point with its distance from the origin. The CSI report for each location is read using MATLAB and at this stage, it needs to be appropriately processed for our ANN.

First, we considered to perform averaging, signal denoising, outlier and redundant removal by applying various technics such as discrete wavelet transform (DWT), Hampel filter, Butterworth filter, principal component analysis (PCA), and extracting seven parameters of the communication link. More specifically we tried 1-D wavelet using Matlab toolbox with Daubechies (db), Symmetric (sym), Coiflets (coif) and Biorthogonal (bior) wavelets for denoising in order to reduce the complexity of our training set patterns and avoid overfitting.

However, during the tests with the processed CSI values, we realized any processing could reduce the richness of our data. So finally, the best idea to organize our data is data expanding instead of removing process. For this purpose, we use all 20 received packets for each location to let our ANN have more training data. As it is previously discussed and shown in fig.4.2, the behaviour of received packets at a specific location is unique and time independent. However, it does not mean all packets are exactly following the same pattern this is why considering 20 packets does not add redundancy. As each packet for a given location is slightly different from the previous and next received packet, we can leverage it to enrich our training set. Finally, to give a comparison between processed and non-processed data we keep the latter technic, i.e. extracting seven parameters as the second scenario.

The CSI values are saved as the matrix of inputs with the number of location multiplied by 20 transmitted packets giving a matrix of 5600 rows and 270 columns for each measurement point. The number 270 represents the nine communication links between pairs of transmitter and receiver antennas multiplied by 30 sub-carriers for each link. We choose two different scenario to train the neural network. In the first approach, all CSI data is used as it is without any further modification as the input for the neural network. In the second approach, seven parameters related to the communication channel are extracted from the CSI data and used as neural network input.

4.6.3. Training the Neural Network

As previously mentioned, we take two approaches in terms of training of our neural network. The use of the CSI data without feature extraction as input in the first one, and as the second approach, inspired by [35], we extract seven parameters related to the communication channel and use them as the inputs of the neural network. The extracted wireless channel parameters are the delay RMS (τ_{rms}), the average delay considering the delay of the first peak as the reference (τ_m), the maximum delay (τ_{max}), the relative total power (P), the number of differentiable multipath corresponding to the detected maximum peaks of the CIR (N), the first element in vector of power amplitudes related to maximum peak (P_1) and the first element in vector of delays related to maximum peaks (τ_1). To use the collected CSIs for ANN training, data processing and normalization is needed. As mentioned before, we consider nine communication links (i.e. the channels between all Tx and Rx antennas) which makes a total of nine, times thirty subcarriers equal to 270 rows. As for each of 280 location, we collect 20 packets our CSI matrix has 5600 columns from which 80% (5600 * 80% = 4480) serve as training data and 20% are used at testing phase. This makes it clear that our approach is regression-based rather than a classification-based approach. Fig. 4.b illustrates the configuration of our system to create the database at the learning phase for two different scenarios of all CSIs and seven extracted parameters.

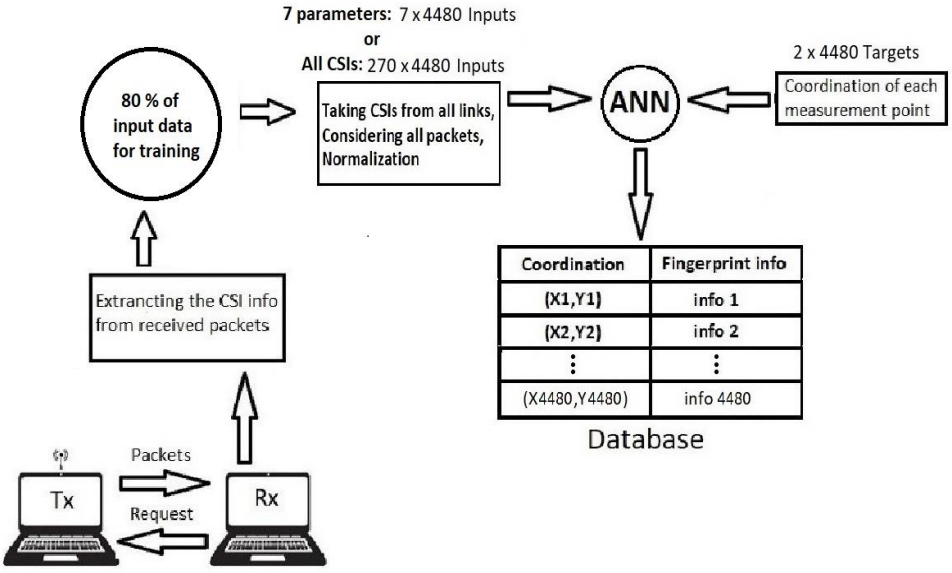

Figure 4. 8 The configuration of our system to create the database at the learning phase

As for ANN, our first network is a feed forward MLP and the second one is a GRNN to perform the regression. For this experiment, we use Multilayer Perceptron (MLP) with one and two layers, and General Regression Neural Network (GRNN) with two different spread factor to get the minimum localization error.

All ANNs are trained with 80% of the database as training data. For the first case, we consider two MLP networks. One with 1 layer and 50 neurons and the other with 2 layers and 50 neurons at the first layer and 24 at the second layer, which prove to be the optimized values for network performance. We set the performance goal at 10^{-4}, the activation function for all layers as tangent sigmoid, mean squared error (MSE) as the loss function, 200 iterations and the Levenberg–Marquardt as the optimization function for nonlinear curve-fitting problems to update weights and biases.

For the second case, GRNN is considered with two different spread factors 1.4 and 1.2. The values for spread factor are selected with trial and error and these two in our experiment show better results in terms of the minimum localization error. Then at the testing phase, ANN preforms the location estimation with 20% of the database as testing data. The cumulative density function of localization error, which is the difference between the actual and the estimated location, together with the performance report is presented in the section 4.6.1.

4.7. Online Phase

In the online phase, the localization is done for 20% of measurements, which are unknown to ANNs. Similar to training phase and considering two previously explained scenario, 20 packets of CSI measures per location or the extracted parameters of 56 (20%*280) test points, depending on the scenario, are fed into two different configuration of ANN: MLP and GRNN.

The trained ANN with the optimized weights and biases estimates the corresponding location to each measurement. Fig. 4.9 illustrates the configuration of our system at the test phase for two different scenarios of all CSIs and seven extracted parameters. Since we have 20 packets of CSI for 56 test points, the total number of inputs and output is 1120.

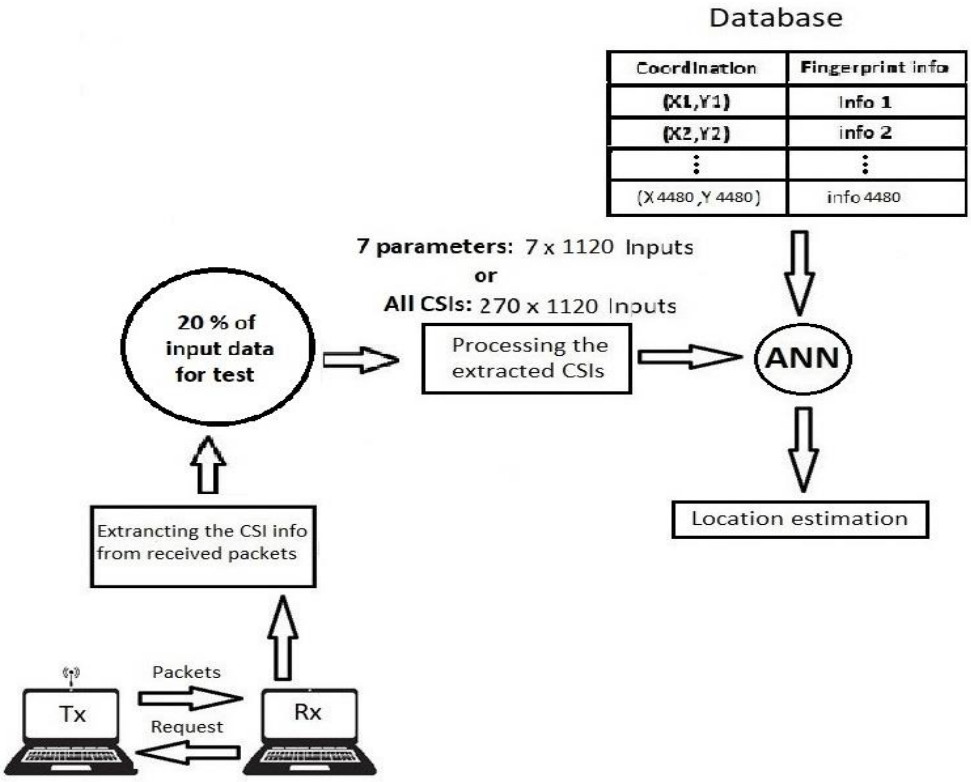

Figure 4. 9 The configuration of our system to create the database at the test phase

4.7.1. Experimental Results

In this section, we present the results for two scenarios and two ANN configurations, as cumulative distribution function (CDF) of localization error with the related analysis of accuracy to give an insight into the system performance.

The results of all the considered cases are given in fig. 4.10 to fig. 4.13. In each figure the error of localization at training and test phase is presented in direction x, y, and the Euclidian distance d. This latter, is the performance index of our system, based on which, we decide the accuracy of each configuration.

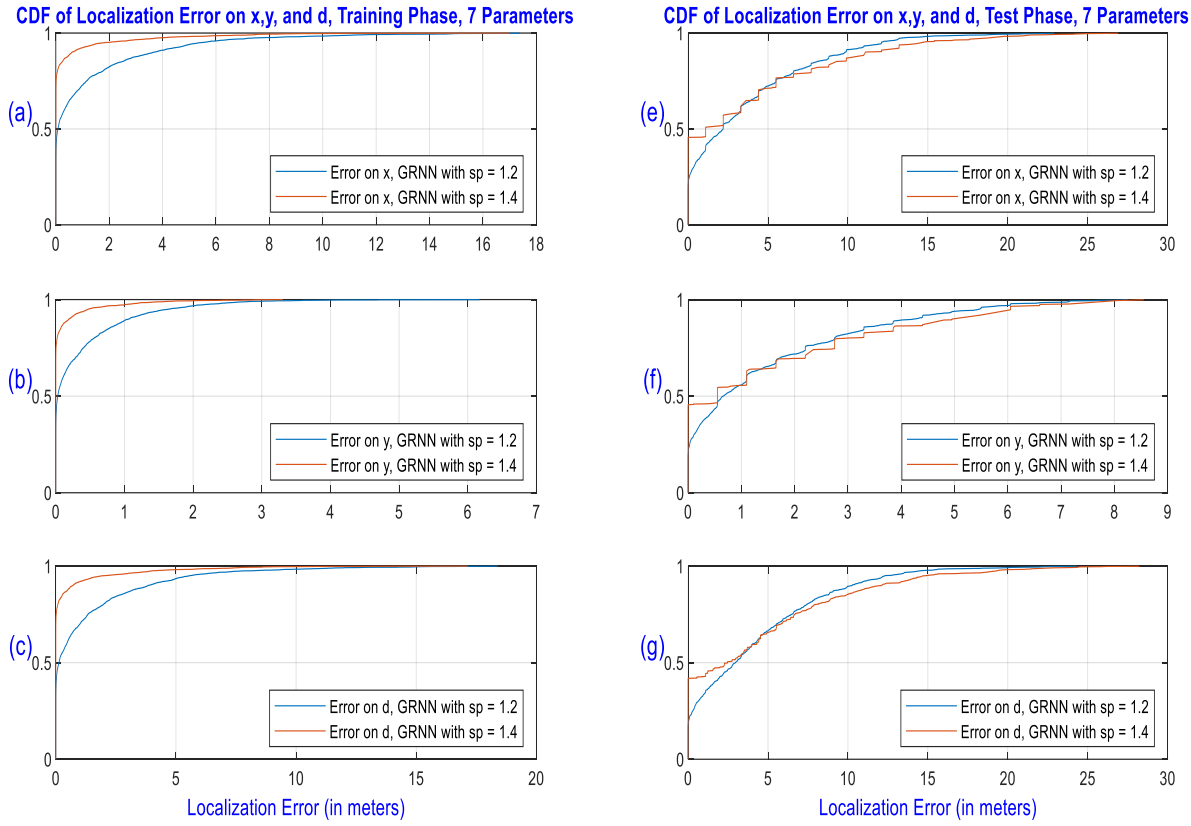

Figure 4. 10 CDF of error for GRNN with spread factor: 1.2, 1.4 and 7extracted parameters.

a: CDF of Error on x, **b:** CDF of Error on y, **c:** CDF of Error on d at training phase.

e: CDF of Error on x, **f:** CDF of Error on y, **g:** CDF of Error on d (Euclidian distance) at testing phase.

As it can be seen from [fig.4.10] (a, b, and c), GRNN network shows a better performance at learning. [Fig 4.10 c] illustrates that around 70% and 90% of locations are learned with less than a meter localization error for spread factor 1.4, and 1.2 respectively. While at the test phase, we observe a dramatic performance drop of around 50% for both spread factors shown in [fig.4.10 g]. Technically, GRNN fails to perform an acceptable estimation with seven extracted parameters as its input. The reason for this lies potentially in the fact that CSI data is already a sampled version

of CFR and by feature extraction; we are actually losing valuable data to the point that even with data augmentation our ANN lacks enough input data to properly train itself.

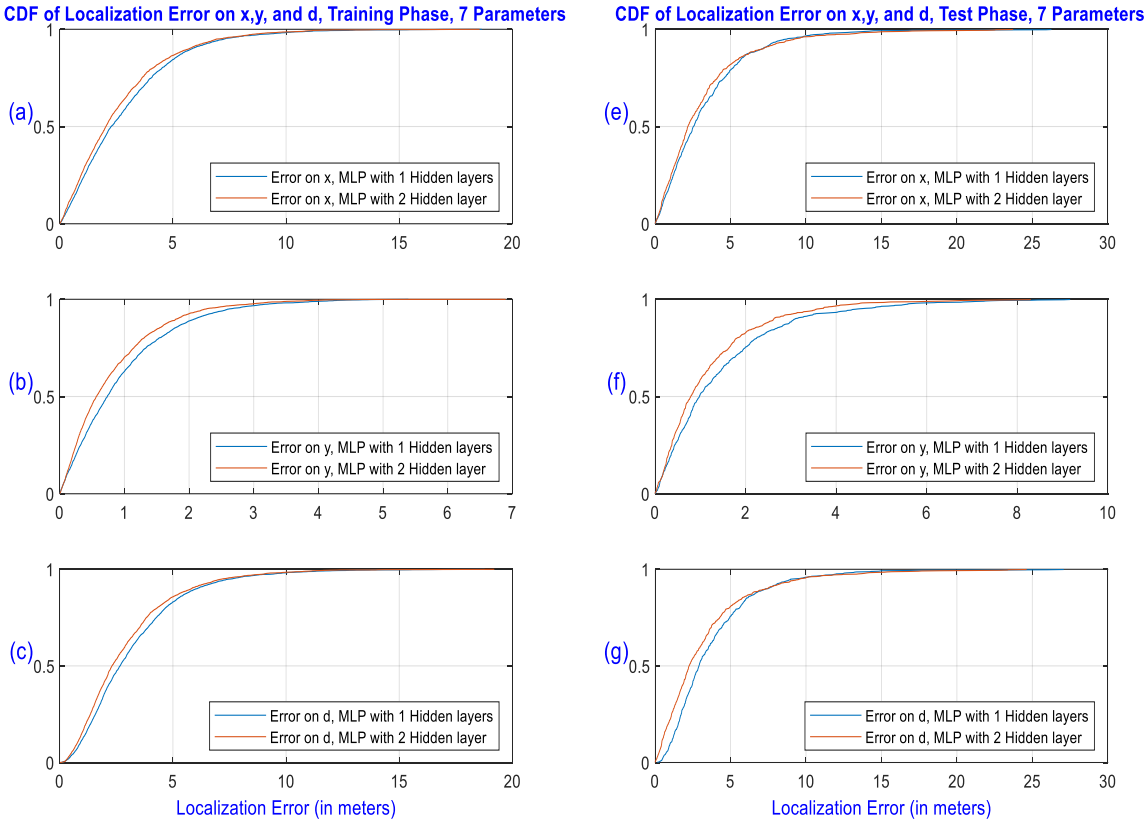

Figure 4. 11 CDF of error for MLP with one hidden layer vs MLP with two hidden layers and 7extracted parameters.

a: CDF of Error on x, **b:** CDF of Error on y, **c:** CDF of Error on d at training phase.

e: CDF of Error on x, **f:** CDF of Error on y, **g:** CDF of Error on d (Euclidian distance) at testing phase.

According to [fig.4.11 c] both one-layered and two-layered MLP compared to GRNN, demonstrate a weaker performance at training phase by around 30% of learned locations with a sub meter error. The results at the test phase, as logically expected are worse with 12% and 16% of learned locations with less than a meter error for one-layered and two-layered MLP, respectively. Quite similar to GRRN, MLP shows a poor performance with seven extracted parameters as its inputs. Therefore, an alternative type of ANN is not a solution to this problem but a richer input data set as it is presented in coming pages boosts the performance of our system.

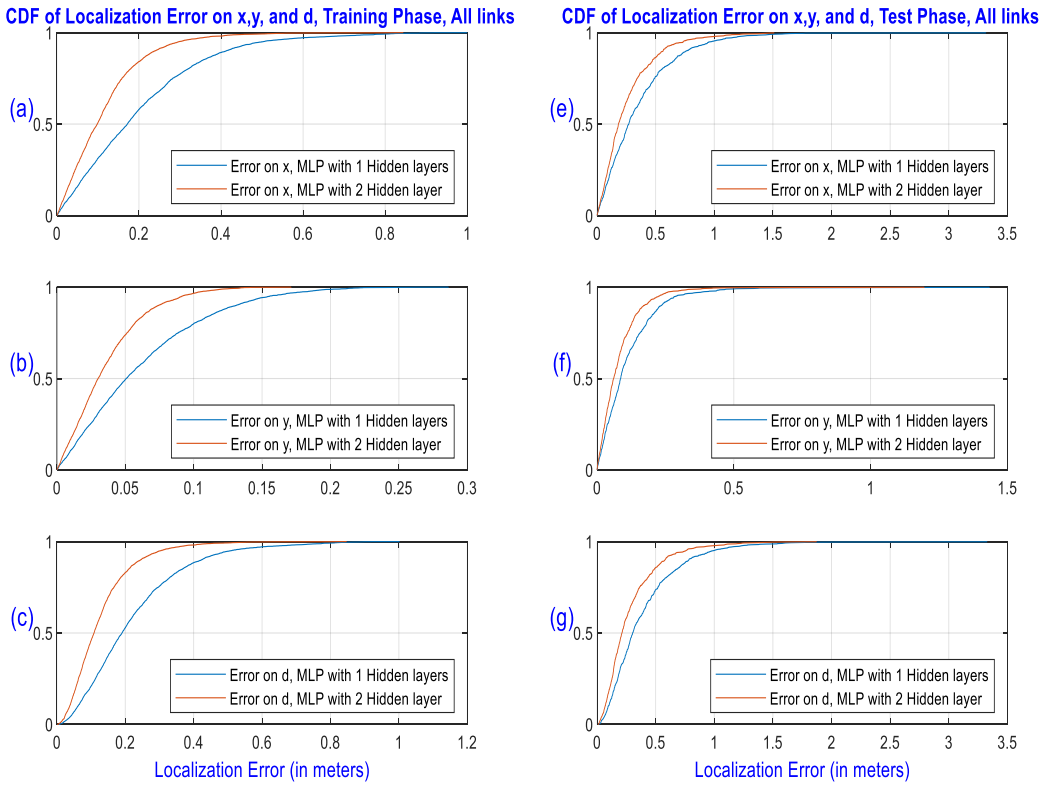

Figure 4. 12 CDF of error for MLP with one hidden layer vs MLP with two hidden layers and all CSIs.

a: CDF of Error on x, **b:** CDF of Error on y, **c:** CDF of Error on d at training phase.

e: CDF of Error on x, **f:** CDF of Error on y, **g:** CDF of Error on d (Euclidian distance) at testing phase.

As discussed previously, we take the normalized CSI data for 20 packets per location and pass it into our ANN without any feature extraction. The CDF of localization error in [fig. 4.12 c] shows a higher location learning accuracy for MLP with two hidden layers. We observe almost 100% of learned locations with less than 0.5 meter error for two-layered MLP while for one-layered MLP the error is around 0.7 meter for 100% of learned locations. Although, the accuracy at test phase is lower [fig.4.12 g], we see that our system achieves a sub meter error for more than 90% and almost 100% of its estimations using one-layered and two-layered MLP, respectively. With closer look at the red curve in [fig. 4.12 g], we see more than 97.7% of the location estimations have been done with less than a meter of localization error, which reveals that MLP with two hidden layers has 2.7% better performance than that of MLP with one hidden layer by

95% successful estimations. The gap between 1-layerd and 2-layered MLP is clearly observable if we consider the number of successful estimations with less than 0.5-meter localization error. For 1-layered MLP 74% and for 2-layered MLP 86% of estimations with less than 0.5-meter shows 12% higher accuracy of 2-layered MLP. It can also be seen that error in X direction is more than error in Y direction, which is reasonable because of 110 cm distance between measurement points on X-axis and 55 cm on Y-axis. As can be seen in Fig.4.12 e and f, both one and two layered configurations reach 100% percent accuracy with less than 0.5 meter localization error in y direction while, for x direction this is not the case having nearly 100% of successful estimation with less than 1-meter error.

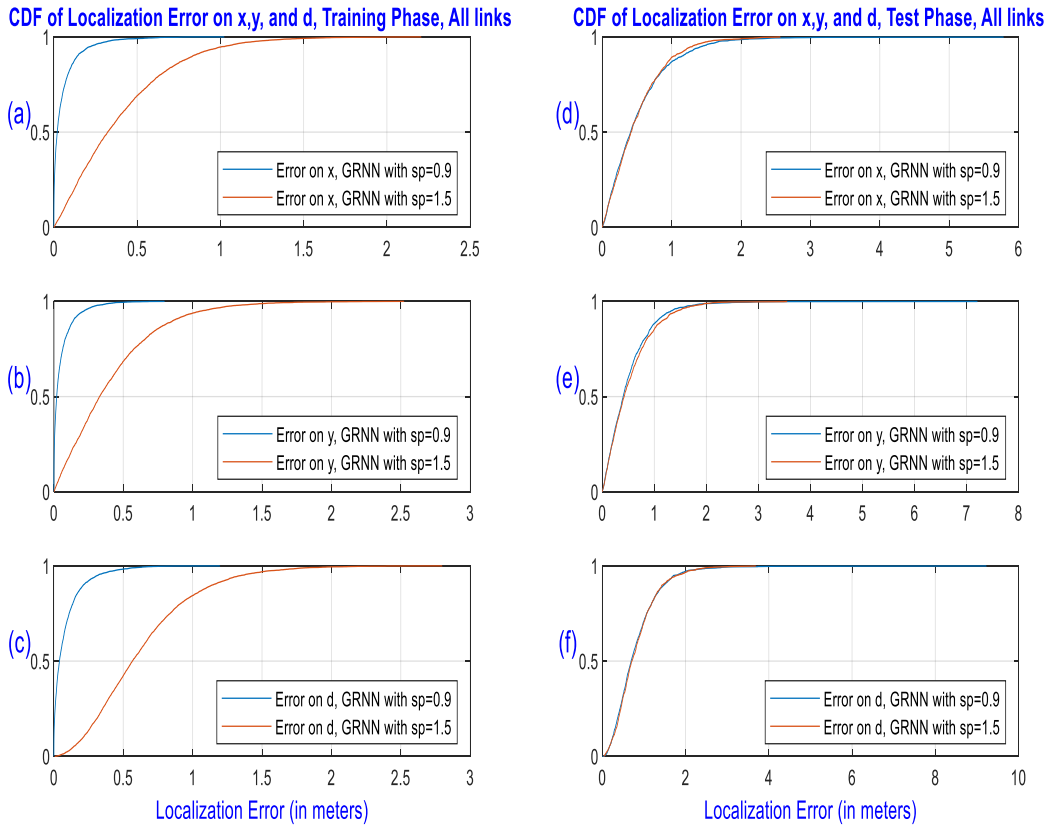

Figure 4. 13 CDF of error for GRNN and all CSIs

a: CDF of Error on x, b: CDF of Error on y, c: CDF of Error on d at training phase.

e: CDF of Error on x, f: CDF of Error on y, g: CDF of Error on d (Euclidian distance) at testing phase.

Fig. 4.13 c clearly illustrates the good learning capability of GRNN at training phase with less than a meter error for 80% and 100% of estimations for spread factor 1.5 and 0.9 respectively.

However, its performance at the test phase [fig. 4.13 d, e and f] is not excellent. The system is trained and tested with 2 different spread factors and the spread factor 0.9, proves to be the optimized setting for GRNN at training phase. The results related to GRNN with the spread factor of 1.5, shows 50% of learned points with less than 0.57 meter and 84% of trained points with less than a meter error. On the other hand, GRNN with spread factor 0.9, at training phase reaches a localization error of 0.10 m for more than 90% of estimations. The spread factor 0.9 clearly improves the GRNN in the learning phase however, as it can be clearly seen the two spread factors show an identical effect on the test phase and no significant difference is observed.

4.7.2. The Effect of ANN Tuning Parameters

We tried various values for the number of layers, neurons, and spread factor. The configuration of a one-layered MLP with 50 neurons and a two-layered MLP with 50 neurons at the first hidden layer and 24 at the second hidden layer give the best results for MLP using both feature-extracted and non feature-extracted scenario. On the other hand, for GRNN, we experienced different pairs of values for two aforementioned scenarios. Table 4.2 and 4.3 summarize the results.

Table 4. 2 Successful estimations with less than 1 m in direction x, y and d, at training phase

Successful estimations with less than 1 m error in:		x	y	d
7 extracted parameters	MLP-1L	16%	19%	11%
	MLP-2L	18%	23%	17%
	GRNN-1.2	75%	90%	68%
	GRNN-1.4	90%	92%	89%
All CSIs	MLP-1L	100%	100%	100%
	MLP-2L	100%	100%	100%
	GRNN-1.5	100%	100%	100%
	GRNN-0.9	92%	90%	81%

Table 4. 3 Successful estimations with less than 1 m in direction x, y and d, at test phase

Under 1-meter successful estimations in:		x	y	d
7 extracted parameters	MLP-1L	24%	25%	17%
	MLP-2L	25%	26%	23%
	GRNN-1.2	35%	34%	21%
	GRNN-1.4	48%	48%	41%
All CSIs	MLP-1L	93%	100%	90%
	MLP-2L	97%	100%	96%
	GRNN-1.5	90%	86%	75%
	GRNN-0.9	88%	90%	75%

CHAPTER 5 CONCLUSION

In this research, we have investigated and compared the efficiency of two different configuration of ANN to localize a mobile user with the fingerprinting technique using CSI data collected over nine communication links. We adopted, MLP and GRNN as our ANN configurations and two scenarios: with and without feature extraction. For the first scenario, seven parameters related to the communication channel are extracted from 20 normalized CSI packets per location and for the second one CSI 20 packets are fed into our ANN without further processing.

For MLP configuration, we compared the effect of one and two hidden layers with 50 and 50-24 neurons respectively, on the functionality of our localization system. Based on our results, a 2-layered MLP with all CSI data as its input shows a better performance of up to 10% over one-layered MLP. The similar results for the case of feature extracted CSI is true, however, since the overall accuracy is considerably degraded after feature extraction, changing the number of layers and neurons does not improve its performance considerably.

As for GRNN, two different spread factors are tried. According to our results, spread factor of 1.4 and 0.9, for feature-extracted and non feature-extracted respectively, improves the accuracy of our system at the training phase while, at the test phase no considerable difference can be seen.

The results show that MLP performs with a considerably higher accuracy of around 24% comparing to GRNN using all CSI information. As it is mentioned, the size of steps between reference points also has an obvious effect on the accuracy of the system, as the error of localization in the y direction is lower than that of the x direction.

Future Work

As an improvement in the future, work, 3-D localization is considered. For this purpose, some modifications are needed such as using external antennas to make sure manies talk to each other on different floors. In addition, our database needs a z-column in coordinate data, which will not be continuous but specific ranges of height will be represented by the floor height. Furthermore, since carrying, an extra device is troublesome in a workplace such as a building; a device-free approach combined with our idea of augmented inputs is suggested for the future work. Moreover,

instead of regression, we may divide the whole area into 1x1 squares and define each of them as a class. The fingerprinting database can be build up using the difference between presence and absence of a human in an area and its effect on CSI amplitude. Another point in to consider in the future work, is implementing multiple transmitter to cover a wider area.

The idea of localization using CSI data can also be used in online tracking of the target. For this purpose, the target should constantly send messages for the server to perform online localization and a user graphic interface could show the movement of the target. The challenge for this idea is higher power consumption, which can be addressed by using more power station supply the device.

REFERENCES

[1] Thoen, B., Wielandt, S., & De Strycker, L. (2018, September). Fingerprinting Method for Acoustic Localization Using Low-Profile Microphone Arrays. In 2018 International Conference on Indoor Positioning and Indoor Navigation (IPIN) (pp. 1-7). IEEE.

[2] Leonardo, R., Barandas, M., & Gamboa, H. (2018). A framework for infrastructure-free indoor localization based on pervasive sound analysis. IEEE Sensors Journal, 18(10), 4136-4144.

[3] Rishabh, I., Kimber, D., & Adcock, J. (2012, November). Indoor localization using controlled ambient sounds. In 2012 International Conference on Indoor Positioning and Indoor Navigation (IPIN) (pp. 1-10). IEEE.

[4] Want, R., Hopper, A., Falcao, V., & Gibbons, J. (1992). The active badge location system. ACM Transactions on Information Systems (TOIS), 10(1), 91-102.

[5] Vidal, J., & Lin, C. Y. (2016, June). Simple and robust localization system using ceiling landmarks and infrared light. In 2016 12th IEEE international conference on control and automation (ICCA) (pp. 583-587). IEEE.

[6] Wang, K., Song, T., Liang, T., Nirmalathas, A., Lim, C., Alameh, K., & Skafidas, E. (2017, March). A dual-infrared-transmitter optical wireless based indoor user localization system with high accuracy. In 2017 Optical Fiber Communications Conference and Exhibition (OFC) (pp. 1-3). IEEE.

[7] Zhang, M., Wen, Y., Chen, J., Yang, X., Gao, R., & Zhao, H. (2018). Pedestrian dead-reckoning indoor localization based on OS-ELM. IEEE Access, 6, 6116-6129.

[8] Kang, W., & Han, Y. (2014). SmartPDR: Smartphone-based pedestrian dead reckoning for indoor localization. IEEE Sensors journal, 15(5), 2906-2916.

[9] Puyol, M. G., Bobkov, D., Robertson, P., & Jost, T. (2014). Pedestrian simultaneous localization and mapping in multistory buildings using inertial sensors. IEEE Transactions on Intelligent Transportation Systems, 15(4), 1714-1727.

[10] Yilmaz, A., & Gupta, A. (2016, October). Indoor positioning using visual and inertial sensors. In 2016 IEEE SENSORS (pp. 1-3). IEEE.

[11] Liu, D., Yang, L., Yu, R., & Liu, Y. (2018, December). GeoLoc: A Geomagnetic Indoor Localization Algorithm with Iterative Uncertainty Elimination. In 2018 14th International Conference on Mobile Ad-Hoc and Sensor Networks (MSN) (pp. 193-198). IEEE.

[12] Yang, S. J., Kim, T. K., Kuc, T. Y., & Park, J. K. (2017, February). Geomagnetic localization of mobile robot. In 2017 IEEE International Conference on Mechatronics (ICM) (pp. 123-127). IEEE.

[13] Zhang, J., & Pan, K. (2015, August). Ultrasound/DR integrated localization and pose tracking for an Indoor Mobile Robot. In 2015 IEEE International Conference on Information and Automation (pp. 847-851). IEEE.

[14] Ens, A., Reindl, L. M., Bordoy, J., Wendeberg, J., & Schindelhauer, C. (2014, October). Unsynchronized ultrasound system for TDOA localization. In 2014 International Conference on Indoor Positioning and Indoor Navigation (IPIN) (pp. 601-610). IEEE.

[15] Hammoud, A., Deriaz, M., & Konstantas, D. (2016, November). Robust ultrasound-based room-level localization system using cots components. In 2016 Fourth international conference on ubiquitous positioning, indoor navigation and location based services (UPINLBS) (pp. 11-19). IEEE.

[16] Chen, C., He, Z., Huang, K., Hu, J., Liu, B., Huang, Q., ... & Xu, H. (2017, October). Visible light communication using the microphone jack of the smart phone as an optical receiver and its application in the indoor localization system. In 2017 International Conference on Electron Devices and Solid-State Circuits (EDSSC) (pp. 1-2). IEEE.

[17] Li, J., Guo, M., & Li, S. (2017, April). An indoor localization system by fusing smartphone inertial sensors and bluetooth low energy beacons. In 2017 2nd International Conference on Frontiers of Sensors Technologies (ICFST) (pp. 317-321). IEEE.

[18] Hou, X., Arslan, T., & Gu, J. (2017, June). Indoor localization for Bluetooth low energy using wavelet and smoothing filter. In 2017 International Conference on Localization and GNSS (ICL-GNSS) (pp. 1-6). IEEE.

[19] Hou, X., Arslan, T., & Gu, J. (2017, June). Indoor localization for Bluetooth low energy using wavelet and smoothing filter. In 2017 International Conference on Localization and GNSS (ICL-GNSS) (pp. 1-6). IEEE.

[20] Wu, J., Zhu, M., Xiao, B., & Qiu, Y. (2018, December). The Improved Fingerprint-Based Indoor Localization with RFID/PDR/MM Technologies. In 2018 IEEE 24th International Conference on Parallel and Distributed Systems (ICPADS) (pp. 878-885). IEEE.

[21] Monica, S., & Ferrari, G. (2015). UWB-based localization in large indoor scenarios: Optimized placement of anchor nodes. IEEE Transactions on Aerospace and Electronic Systems, 51(2), 987-999.

[22] Ni, D., Postolache, O. A., Mi, C., Zhong, M., & Wang, Y. (2019, March). UWB Indoor Positioning Application Based on Kalman Filter and 3-D TOA Localization Algorithm. In 2019 11th International Symposium on Advanced Topics in Electrical Engineering (ATEE) (pp. 1-6). IEEE.

[23] Yu, F., Jiang, M., Liang, J., Qin, X., Hu, M., Peng, T., & Hu, X. (2014, April). An indoor localization of WiFi based on branch-bound algorithm. In 2014 International Conference on Information Science, Electronics and Electrical Engineering (Vol. 2, pp. 1306-1308). IEEE.

[24] Salamah, A. H., Tamazin, M., Sharkas, M. A., & Khedr, M. (2016, October). An enhanced WiFi indoor localization system based on machine learning. In 2016 International Conference on Indoor Positioning and Indoor Navigation (IPIN) (pp. 1-8). IEEE.

[25] Bahl, P., Padmanabhan, V. N., Bahl, V., & Padmanabhan, V. (2000). RADAR: An in-building RF-based user location and tracking system.

[26] Bahl, V., & Padmanabhan, V. (2000). Enhancements to the RADAR user location and tracking system.

[27] Golden, S. A., & Bateman, S. S. (2007). Sensor measurements for Wi-Fi location with emphasis on time-of-arrival ranging. IEEE Transactions on Mobile Computing, 6(10), 1185-1198.

[28] Makki, A., Siddig, A., Saad, M., Cavallaro, J. R., & Bleakley, C. J. (2015). Indoor localization using 802.11 time differences of arrival. IEEE Transactions on Instrumentation and Measurement, 65(3), 614-623.

[29] Xiong, J., & Jamieson, K. (2013). Arraytrack: A fine-grained indoor location system. In Presented as part of the 10th {USENIX} Symposium on Networked Systems Design and Implementation ({NSDI} 13) (pp. 71-84).

[30] Kotaru, M., Joshi, K., Bharadia, D., & Katti, S. (2015, August). Spotfi: Decimeter level localization using wifi. In ACM SIGCOMM computer communication, review (Vol. 45, No. 4, pp. 269-282). ACM.

[31] Samadh, S. A., Liu, Q., Liu, X., Ghourchian, N., & Allegue, M. (2019, January). Indoor Localization Based on Channel State Information. In 2019 IEEE Topical Conference on Wireless Sensors and Sensor Networks (WiSNet) (pp. 1-4). IEEE.

[32] Cai, C., Deng, L., & Li, S. (2018, December). CSI-Based Device-Free Indoor Localization Using Convolutional Neural Networks. In 2018 IEEE 4th International Conference on Computer and Communications (ICCC) (pp. 753-757). IEEE.

[33] Rai, A., Chintalapudi, K. K., Padmanabhan, V. N., & Sen, R. (2012, August). Zee: Zero-effort crowdsourcing for indoor localization. In Proceedings of the 18th annual international conference on Mobile computing and networking (pp. 293-304). ACM.

[34] Sen, S., Radunovic, B., Choudhury, R. R., & Minka, T. (2012, June). You are facing the Mona Lisa: Spot localization using PHY layer information. In Proceedings of the 10th international conference on Mobile systems, applications, and services (pp. 183-196). ACM.

[35] Nerguizian, Chahé, Charles Despins, and Sofiène Affès. "Geolocation in mines with an impulse response fingerprinting technique and neural networks." IEEE Transactions on Wireless Communications 5, no. 3 (2006): 603-611.

[36] Halperin, D., Hu, W., Sheth, A., & Wetherall, D. (2011). Tool release: Gathering 802.11 n traces with channel state information. ACM SIGCOMM Computer Communication Review, 41(1), 53-53.

[37] Wu, K., Xiao, J., Yi, Y., Gao, M., & Ni, L. M. (2012, March). Fila: Fine-grained indoor localization. In 2012 Proceedings IEEE INFOCOM (pp. 2210-2218). IEEE.

[38] Xiao, J., Wu, K., Yi, Y., & Ni, L. M. (2012, July). FIFS: Fine-grained indoor fingerprinting system. In 2012 21st international conference on computer communications and networks (ICCCN) (pp. 1-7). IEEE.

[39] Sen, S., Lee, J., Kim, K. H., & Congdon, P. (2013, June). Avoiding multipath to revive inbuilding WiFi localization. In Proceeding of the 11th annual international conference on Mobile systems, applications, and services (pp. 249-262). ACM.

[40] Xiao, J., Wu, K., Yi, Y., Wang, L., & Ni, L. M. (2013, July). Pilot: Passive device-free indoor localization using channel state information. In 2013 IEEE 33rd International Conference on Distributed Computing Systems (pp. 236-245). IEEE.

[41] Xiao, J., Wu, K., Yi, Y., Wang, L., & Ni, L. M. (2013, July). Pilot: Passive device-free indoor localization using channel state information. In 2013 IEEE 33rd International Conference on Distributed Computing Systems (pp. 236-245). IEEE.

[42] Wang, X., Gao, L., & Mao, S. (2015, December). PhaseFi: Phase fingerprinting for indoor localization with a deep learning approach. In 2015 IEEE Global Communications Conference (GLOBECOM) (pp. 1-6). IEEE.

[43] Wang, X., Gao, L., Mao, S., & Pandey, S. (2016). CSI-based fingerprinting for indoor localization: A deep learning approach. IEEE Transactions on Vehicular Technology, 66(1), 763-776.

[44] Wang, J., Zhang, L., Wang, X., Xiong, J., Chen, X., & Fang, D. (2016, October). A novel CSI pre-processing scheme for device-free localization indoors. In Proceedings of the Eighth Wireless of the Students, by the Students, and for the Students Workshop (pp. 6-8). ACM.

[45] Alibi, D., Javed, U., Wen, F., He, D., Liu, P., Zhang, Y., & Jiang, L. (2016, November). 2D DOA estimation method based on channel state information for uniform circular array. In 2016 Fourth International Conference on Ubiquitous Positioning, Indoor Navigation and Location Based Services (UPINLBS) (pp. 68-72). IEEE.

[46] Jiang, W., Liu, Y., Lei, Y., Wang, K., Yang, H., & Xing, Z. (2017, June). For better CSI fingerprinting based localization: a novel phase sanitization method and a distance metric. In 2017 IEEE 85th Vehicular Technology Conference (VTC Spring) (pp. 1-7). IEEE.

[47] Wang, X., Wang, X., & Mao, S. (2017, May). CiFi: Deep convolutional neural networks for indoor localization with 5 GHz Wi-Fi. In 2017 IEEE International Conference on Communications (ICC) (pp. 1-6). IEEE.

[48] Chen, H., Zhang, Y., Li, W., Tao, X., & Zhang, P. (2017). ConFi: Convolutional neural networks based indoor Wi-Fi localization using channel state information. IEEE Access, 5, 18066-18074.

[49] Escudero, G., Hwang, J. G., & Park, J. G. (2017). An indoor positioning method using ieee 802.11 channel state information. Journal of Electrical Engineering & Technology, 12(3), 1286-1291.

[50] Wu, G. S., & Tseng, P. H. (2018, March). A deep neural network-based indoor positioning method using channel state information. In 2018 International Conference on Computing, Networking and Communications (ICNC) (pp. 290-294). IEEE.

[51] Sanam, T. F., & Godrich, H. (2018, September). An Improved CSI Based Device Free Indoor Localization Using Machine Learning Based Classification Approach. In 2018 26th European Signal Processing Conference (EUSIPCO) (pp. 2390-2394). IEEE.

[52] Ahmed, A. U., Bergmann, N. W., Arablouei, R., Kusy, B., De Hoog, F., & Jurdak, R. (2018, April). Fast indoor localization using WiFi channel state information. In 2018 17th ACM/IEEE International Conference on Information Processing in Sensor Networks (IPSN) (pp. 120-121). IEEE.

[53] Cai, C., Deng, L., Zheng, M., & Li, S. (2018, March). PILC: Passive Indoor Localization Based on Convolutional Neural Networks. In 2018 Ubiquitous Positioning, Indoor Navigation and Location-Based Services (UPINLBS) (pp. 1-6). IEEE.

[54] Xiang, C., Zhang, Z., Zhang, S., Xu, S., Cao, S., & LAU, V. (2019). Robust Sub-meter Level Indoor Localization-A Logistic Regression Approach. arXiv preprint arXiv:1902.06226.

[55] Zhang, L., Ding, E., Hu, Y., & Liu, Y. (2019). A novel CSI-based fingerprinting for localization with a single AP. EURASIP Journal on Wireless Communications and Networking, 2019(1), 51.

[56] Hsieh, C. H., Chen, J. Y., & Nien, B. H. (2019). Deep Learning-Based Indoor Localization Using Received Signal Strength and Channel State Information. IEEE Access, 7, 33256-33267.

[57] Wu, Z., Xu, Q., Li, J., Fu, C., Xuan, Q., & Xiang, Y. (2017). Passive indoor localization based on csi and naive bayes classification. IEEE Transactions on Systems, Man, and Cybernetics: Systems, 48(9), 1566-1577.

[58] Deng, Z., Fu, X., Cheng, Q., Shi, L., & Liu, W. (2019). CC-DTW: An Accurate Indoor Fingerprinting Localization Using Calibrated Channel State Information and Modified Dynamic Time Warping. Sensors, 19(9), 1984.

[59] 802.11n-2009 - IEEE Standardfor Information technology-- Local and metropolitan area networks-- Specific requirements-- Part 11: Wireless LAN Medium Access Control (MAC) and Physical Layer (PHY) Specifications Amendment 5: Enhancements for Higher Throughput

[60] https://dhalperi.github.io/linux-80211n-csitool/installation.html

[61] https://towardsdatascience.com/

APPENDIX A

After installing the Intel WiFi Link 5300 NIC and first Ubuntu 14.04.5 LTS 32-bit on both laptops, kernel-packagefollowing codes in the Ubuntu terminal:

1. First step (Essentials)

These lines of code install the build tools, the Linux development headers, and the Git client. Also, based on the installation instructions it is advised to disable Network Manager, so that it will not control the wireless card while we run the experiment:

```
sudo apt-get install gcc make linux-headers-$(uname -r) git-core
sudo apt-get install iw
echo iface wlan0 inet manual | sudo tee -a /etc/network/interfaces
sudo restart network-manager
```

To make sure the driver will not automatically load during boot run the following lines:

```
echo blacklist iwldvm | sudo tee -a /etc/modprobe.d/csitool.conf
echo blacklist iwlwifi | sudo tee -a /etc/modprobe.d/csitool.conf
```

2. Second step (Modifying the Wireless adaptor Driver)

Next, we need to apply modification to the driver and the correct tag for upstream kernel should be checked by getting the complete information of CSI Tool Linux (Linux source tree):

```
CSITOOL_KERNEL_TAG=csitool-$(uname -r | cut -d . -f 1-2)
git clone https://github.com/dhalperi/linux-80211n-csitool.git
cd linux-80211n-csitool
git checkout ${CSITOOL_KERNEL_TAG}
```

More over the compatibility can be improved by merging the applied modification into the Linux source tree:

```
. /etc/lsb-release
git remote add ubuntu git://kernel.ubuntu.com/ubuntu/ubuntu-${DISTRIB_CODENAME}.git
git pull --no-edit ubuntu ${UBUNTU_KERNEL_TAG}
```

The modified driver can be built for the current kernel:

```
make -C /lib/modules/$(uname -r)/build M=$(pwd)/drivers/net/wireless/iwlwifi modules
```

Consequently, the built driver is installed into the module updates directory:

```
sudo make -C /lib/modules/$(uname -r)/build M=$(pwd)/drivers/net/wireless/iwlwifi
INSTALL_MOD_DIR=updates \   modules_install
sudo depmod
cd ..
```

3. Third step, Installing the Modified Firmware

In this step we need to get the CSI Tool supplementary material by running the following lines:

```
git clone https://github.com/dhalperi/linux-80211n-csitool-supplementary.git
```

Removing the current firmware for Intel Wi-Fi Link 5000 Series adapters:

```
for file in /lib/firmware/iwlwifi-5000-*.ucode; do sudo mv $file $file.orig; done
```

Installing the new firmware (modified):

```
sudo cp linux-80211n-csitool-supplementary/firmware/iwlwifi-5000-2.ucode.sigcomm2010
/lib/firmware/
sudo ln -s iwlwifi-5000-2.ucode.sigcomm2010 /lib/firmware/iwlwifi-5000-2.ucode
```

4. Fourth step, Building the Logging Tool

This command makes it possible to write the obtained CSI to a file:

```
make -C linux-80211n-csitool-supplementary/netlink
```

5. Fifth step, Enabling the Logging and Test

Before loading the driver to log, the current driver must be unloaded:

```
sudo modprobe -r iwlwifi mac80211
```

In case the error message (FATAL: Module iwlwifi is in use) appears." It implies that we must firstly unloade iwldvm module by running the following line:

```
sudo modprobe -r iwldvm iwlwifi mac80211
```

Now the new driver with the ability to log is reloaded:

```
sudo modprobe iwlwifi connector_log=0x1
```

Finally to log CSI to a file:

```
sudo linux-80211n-csitool-supplementary/netlink/log_to_file csi.dat
```

This page contains the codes that are at transmitter and receiver sides to enable injection and monitoring. Running some lines may lead to error messages but they should be ignored.

Transmitter side:

```
cd linux-80211n-csitool-supplementary/injection

sudo modprobe -r iwldvm

sudo modprobe -r iwlwifi mac80211 cfg80211

sudo modprobe iwlwifi

sudo ifup wlan0

sudo modprobe -r iwlwifi mac80211 cfg80211

sudo modprobe iwlwifi debug=0x40000 connector_log=0x1

sudo iwconfig wlan0 mode monitor

sudo iw dev wlan0 interface add mon0 type monitor

sudo iw dev mon0 set channel 64 HT20

sudo ip link set wlan0 down 2>/dev/null 1>/dev/null

sudo iw dev wlan0 set type monitor 2>/dev/null 1>/dev/null

sudo ip link set wlan0 up

sudo iw dev mon0 set channel 64 HT20

sudo find /sys -name monitor_tx_rate

/sys/kernel/debug/iwlwifi/0000:03:00.0/iwldvm/debug/monitor_tx_rate
```

For one transmitter antenna:

```
echo 0x4101 | sudo tee /sys/kernel/debug/iwlwifi/0000:03:00.0/iwldvm/debug/monitor_tx_rate

0x4101
```

For three transmitter antennas:

echo 0x1c113 | sudo tee /sys/kernel/debug/iwlwifi/0000:03:00.0/iwldvm/debug/monitor_tx_rate

0x1c113

mohsen@mohsen-ThinkPad-T61:~/linux-80211n-csitool-supplementary/injection$ sudo ./random_packets 100000 100 1

Receiver Side:

Terminal one:

sudo modprobe -r iwldvm iwlwifi mac80211

sudo modprobe iwlwifi connector_log=0x1

sudo iwconfig wlan0 mode monitor

sudo iw wlan0 set channel 64 HT20

command failed: Device or resource busy (-16)

sudo modprobe iwlwifi

sudo ifup wlan0

sudo iw wlan0 set channel 64 HT20

sudo ifconfig wlan0 up

Terminal 2:

sudo linux-80211n-csitool-supplementary/netlink/log_to_file Desktop/csi.dat